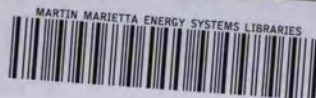


99

MARTIN MARIETTA ENERGY SYSTEMS LIBRARIES



3 4456 0134146 2

CENTRAL RESEARCH LIBRARY
DOCUMENT COLLECTION

ORNL-3503
UC-80 - Reactor Technology
TID-4500 (26th ed.)

DESIGN AND THERMAL ANALYSIS OF
EGCR CONTROL RODS
J. W. Michel

CENTRAL RESEARCH LIBRARY
DOCUMENT COLLECTION
LIBRARY LOAN COPY
DO NOT TRANSFER TO ANOTHER PERSON
If you wish someone else to see this
document, send in name with document
and the library will arrange a loan.



OAK RIDGE NATIONAL LABORATORY
operated by
UNION CARBIDE CORPORATION
for the
U.S. ATOMIC ENERGY COMMISSION

Printed in USA. Price: \$1.50 Available from the
Office of Technical Services
U. S. Department of Commerce
Washington 25, D. C.

— LEGAL NOTICE —

This report was prepared as an account of Government sponsored work. Neither the United States, nor the Commission, nor any person acting on behalf of the Commission:

- A. Makes any warranty or representation, expressed or implied, with respect to the accuracy, completeness, or usefulness of the information contained in this report, or that the use of any information, apparatus, method, or process disclosed in this report may not infringe privately owned rights; or
- B. Assumes any liabilities with respect to the use of, or for damages resulting from the use of any information, apparatus, method, or process disclosed in this report.

As used in the above, "person acting on behalf of the Commission" includes any employee or contractor of the Commission, or employee of such contractor, to the extent that such employee or contractor of the Commission, or employee of such contractor prepares, disseminates, or provides access to, any information pursuant to his employment or contract with the Commission, or his employment with such contractor.

ORNL-3503

Contract No. W-7405-eng-26

Reactor Division

DESIGN AND THERMAL ANALYSIS OF EGCR CONTROL RODS

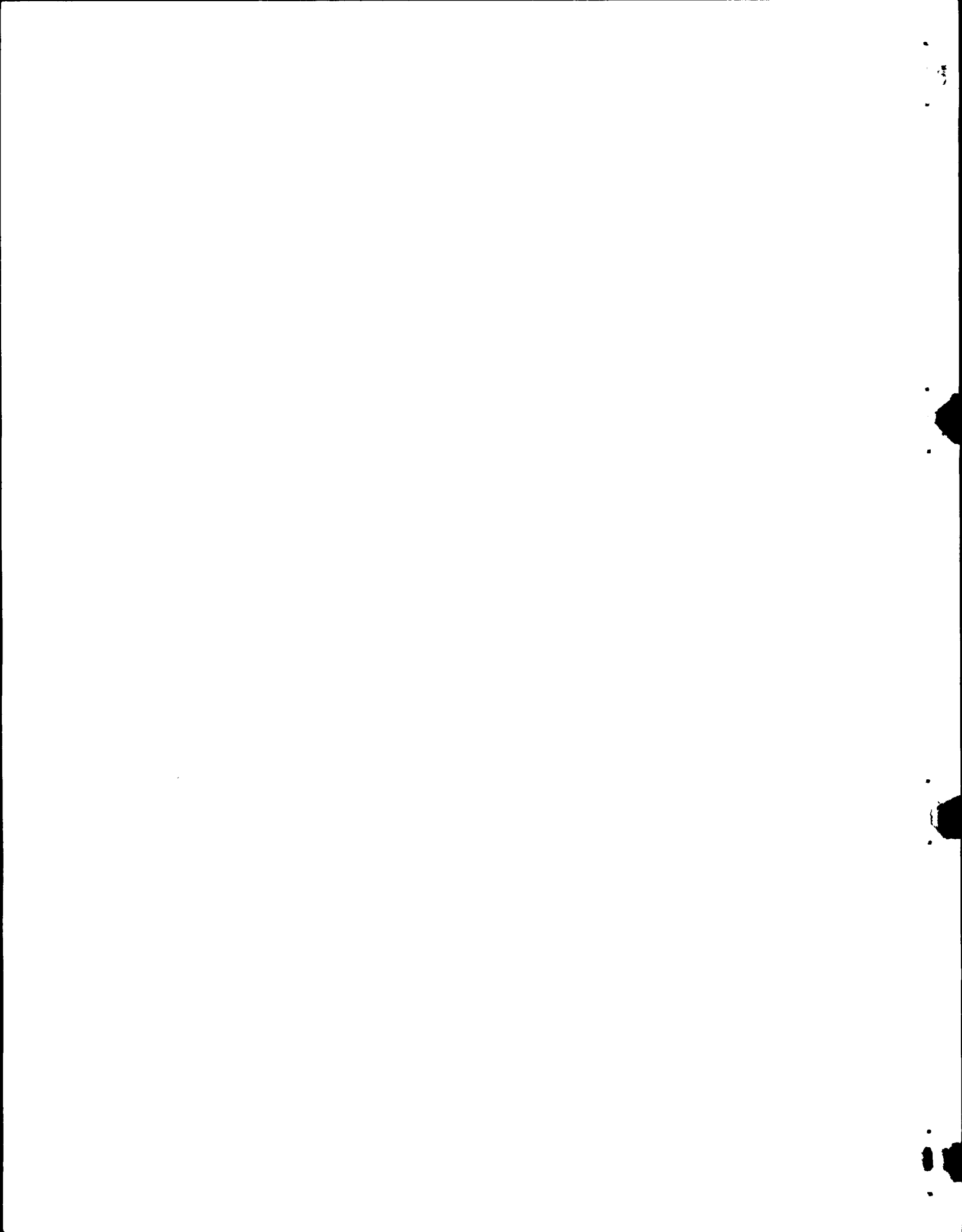
J. W. Michel

MARCH 1964

OAK RIDGE NATIONAL LABORATORY
Oak Ridge, Tennessee
operated by
UNION CARBIDE CORPORATION
for the
U.S. ATOMIC ENERGY COMMISSION

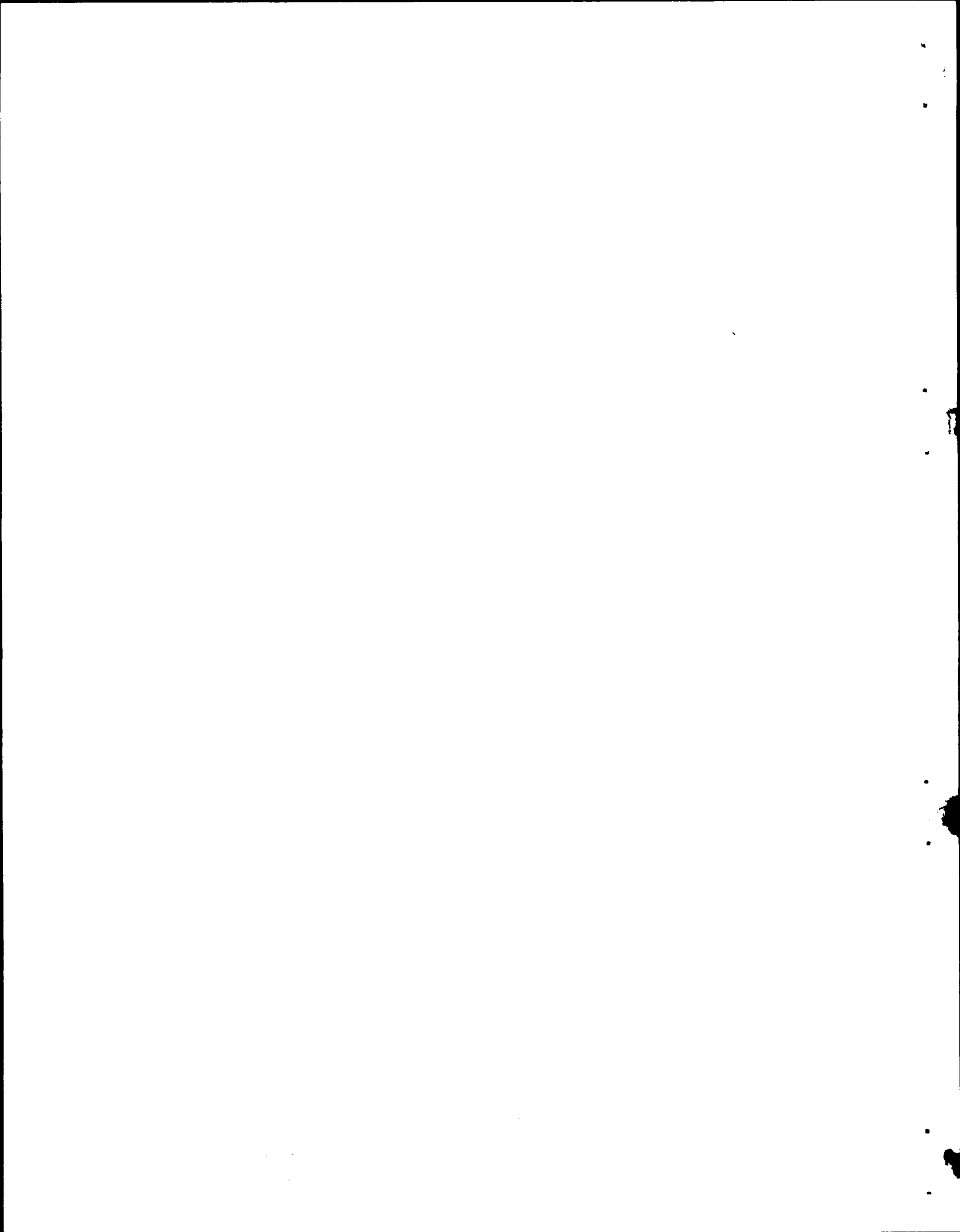


3 4456 0134146 2



CONTENTS

	<u>Page</u>
Abstract	1
Introduction	1
Design Requirements	1
Design Criteria	5
General Description	6
Thermal Considerations	8
Mechanical Considerations	13
Fabrication and Testing of the Mockup Control Rod	14
Production of the EGCR Control Rods	15
References	27
Appendix	29



DESIGN OF CONTROL RODS FOR THE EXPERIMENTAL GAS-COOLED REACTOR

J. W. Michel

ABSTRACT

Control rods were designed for use in the Experimental Gas-Cooled Reactor that are sufficiently flexible to move in bowed graphite channels. The stainless steel-clad B_4C bushings that make up the control rods are suspended on cables connected to the drive mechanisms. The rods are cooled internally by helium admitted at the top of the control rod nozzles. Tests of a mockup of a control rod verified the feasibility of assembly and provided pressure drop data. No major manufacturing problems were encountered and the finished rod weights varied from 137 to 142 lb.

Introduction

The preliminary design of the control rods for the experimental gas-cooled reactor (EGCR) was completed in July 1959 by the Allis-Chalmers Manufacturing Company, and the responsibility for the final design and the purchasing of the rods was transferred to the Oak Ridge National Laboratory at that time. The design and procurement of the control rod shock absorber, a portion of which is attached to the top of the control rod, remained the responsibility of Allis-Chalmers. The initial control rod design consisted of one continuous tube containing boron carbide bushings and was completed before data were available on the shrinkage and consequent bowing of the graphite columns within which the rods were to move. In order to accommodate the shrinkage, design changes were necessary to articulate the rod and to cool it by admitting the coolant to the top inside of the rod instead of to the bottom around the outside.

Design Requirements

The EGCR has 21 control rods placed on 24-in. centers throughout the core, as shown in Fig. 1. The control rod channels are 4 in. in diameter and are located at intersections of graphite columns, except the

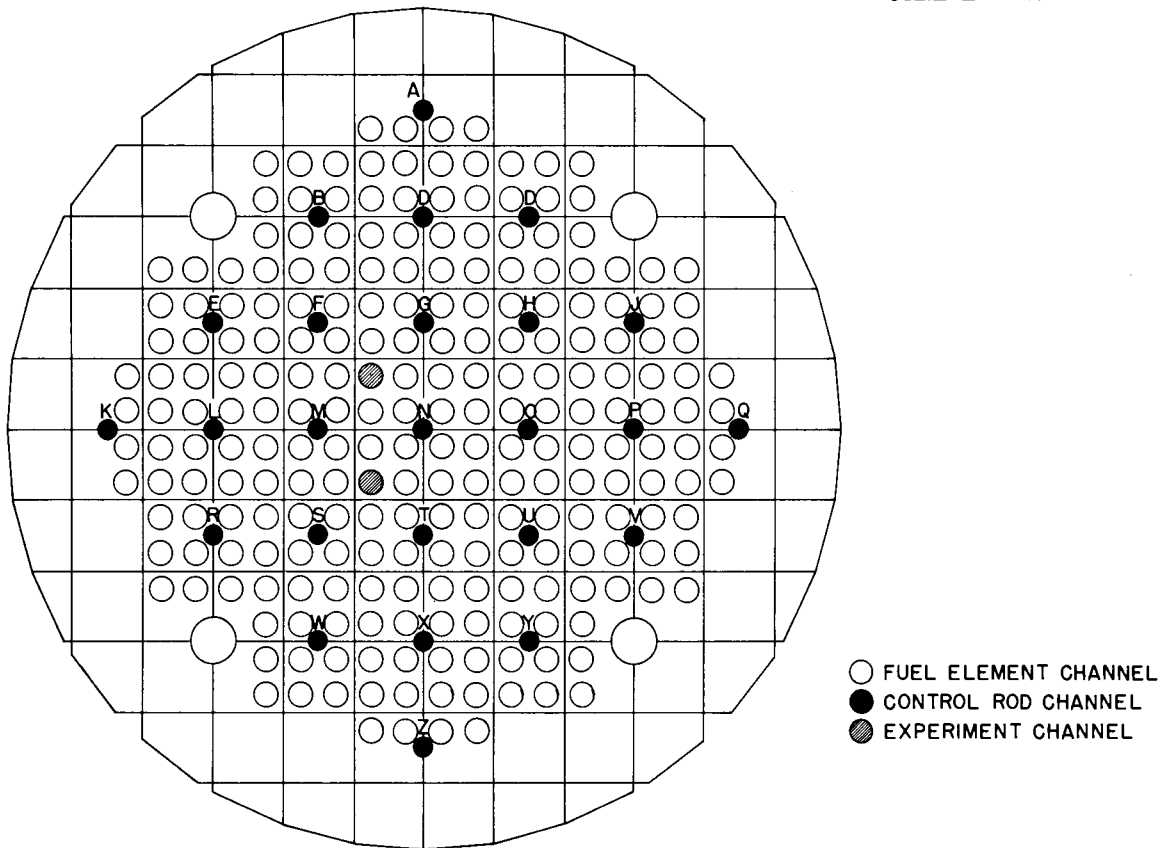


Fig. 1. Plan View of EGCR Moderator.

four channels S, U, F, and H, which are in the center of columns. Based on the EGCR critical experiment and subsequent calculations,¹ it was found that 21 rods 3 1/4 in. in diameter would provide a shutdown worth in the cold reactor of $\Delta k = 0.261$, giving an excess Δk of 0.100 for the cold, clean initial core and 0.174 for the hot, equilibrium condition. Calculations of the reactivity resulting from the withdrawal of individual control rods indicated that any five rods can be withdrawn, or fail to insert, and the reactor will remain subcritical in the initial cold, clean condition.

It is expected that the rods will be operated primarily in banks, with one or more of the centrally located rods being fully inserted for radial flux flattening or to compensate for gross excess reactivity resulting from experimental systems or specimens inserted in the reactor.

The normal rate of movement of the rods will be 1.8 in./min, except that during the "free-fall" portion of a scram the rod will fall under the influence of gravity at an acceleration of approximately 0.6 g until it reaches a velocity of about 18 ft/sec.

The rods are suspended on 3/16-in., type 304 stainless steel, 7 x 10 cables connected to the drive mechanisms located near the top of the control rod nozzles, as shown in Fig. 2. A shroud tube hung from the nozzle guides the rods into the core channels, provides the coolant flow path, and contains the collet portion of the shock absorber. Thus, in the event of a broken cable or a drive failure, the shock load of stopping a free-falling control rod will be transferred to the pressure vessel and thus prevent damage to the core.

The control rod channels will become bowed with time because of non-uniform graphite shrinkage induced by the fast-neutron flux gradient across the core. The restraint bands should limit the maximum bow to about 1 in., but the blocks may eventually crack² and become offset and thus it would be difficult for solid control rods to move readily in and out of the channels. In addition, the channels may become slightly misaligned because of differential thermal expansion and some pressurization effects. For example, the graphite blocks may become tilted because of the higher expansion rate of the top restraint structure, which will operate at a higher temperature than the bottom plate. Consequently, it was established as a design requirement that the rods be sufficiently flexible to move readily in and out of bowed channels made up of cracked graphite columns.

The design requirements also specified that the control rods should be compatible with the reactor environment of helium at a pressure of approximately 300 psia. The helium is expected to contain trace amounts of nitrogen, hydrogen, water, CO, CO₂, and CH₄. The rod cladding material should be compatible with graphite at temperatures up to 1600°F and with both type 304 stainless steel and the nuclear poison.

Further, the rods should be operable during accident conditions and should be of sufficient strength to withstand the shock load resulting from a broken support cable, as well as the loads imposed by the normal

UNCLASSIFIED
ORNL-LR-DWG. 46416R

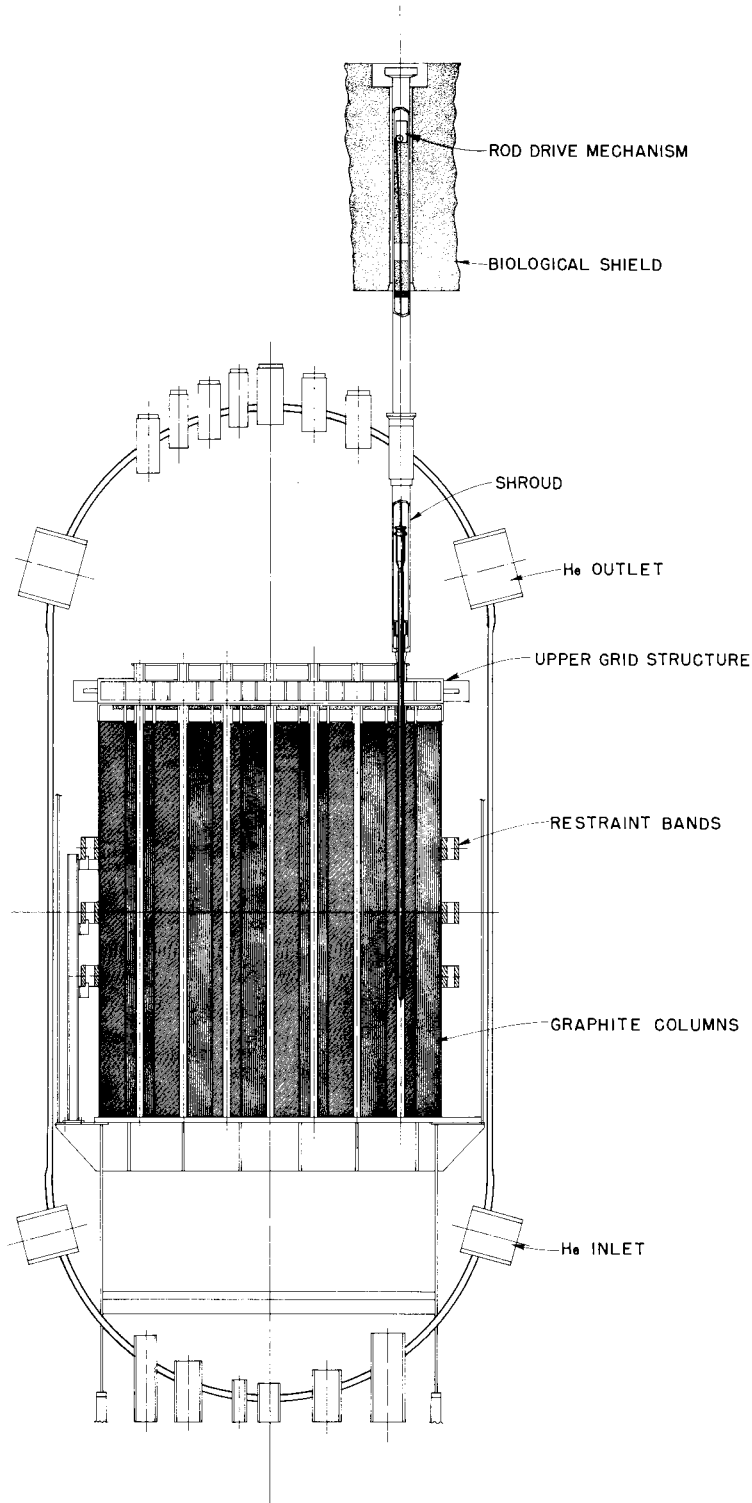


Fig. 2. Vertical Section Through EGCR Core.

thermal and mechanical stresses. The nuclear poison should be contained within the rod throughout the rod lifetime, which was taken to be 20 years.

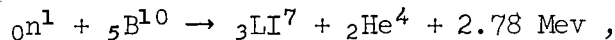
Design Criteria

Boron carbide (B_4C) was chosen as the nuclear poison in the Title-I design³ on the basis of a cost study and a survey of the properties and use of B_4C for this purpose. The Title-I study indicated that boronated (1 1/2% boron) stainless steel would give the lowest initial cost, but the predictable life of this material is short and the nature and extent of radiation damage precluded its use. Its use would also cause the rod weight to be larger and consequently increase the complexity of the rod drives and shock absorbers.

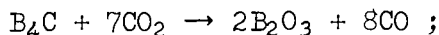
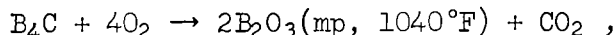
Some of the properties of B_4C that affect control rod design are summarized below:

Neutron cross section (normal B^{10} assay), barns	755
Thermal conductivity, Btu/hr·ft·°F	10.0
Thermal expansion coefficient, per °F	2.5×10^{-6}
Specific gravity	
Theoretical	2.51
Commercial	2.0
Melting point, °F	4440
Compressive strength, psi	410,000

The nuclear reaction is



and the chemical reactions are



also B_2O_3 may react with water vapor to form HBO_2 or H_3BO_3 .

The high thermal-neutron cross section of 755 barns per atom for natural boron and the fact that boron is an ideal $1/v$ absorber make the rods essentially black over a considerable neutron-energy range. The nuclear lifetime for the B_4C in this application is estimated to be about 40 years for a fully inserted control rod.

The thermal conductivity is high enough so that even though essentially all the thermal neutrons are absorbed in the outer layers of the B_4C , its radial temperature distribution will be essentially uniform and hot spots should not be a problem. The heat generated by neutron absorption, as well as by gamma absorption, is removed by forced-convection helium cooling to maintain all rod components within their allowable temperature limits.

Allowances were made for differential thermal expansion, since the stainless steel cladding has a thermal expansion coefficient about four times as high as that of the B_4C . The fact that B_4C will react with air or CO_2 to form B_2O_3 , which has a relatively low melting point, called for special precautions to assure that air, CO_2 , and H_2O do not come into contact with the B_4C at the high operating temperatures.

Helium released from the neutron-absorption reaction does not pose a significant problem, since it can be released into the normal helium coolant stream. The fact that lithium and helium are formed indicates, however, that there may be problems in maintaining the dimensional stability of the B_4C . There has been considerable study of both this point and the amount of helium released,⁴⁻⁸ but somewhat conflicting results have been obtained. One characteristic of boron that required attention was its reaction with nickel and, to a lesser extent, with stainless steel⁹ at elevated temperatures. It was found that copper was an excellent diffusion barrier¹⁰ to prevent this reaction.

General Description

The final design, shown in Fig. 3, specified a control rod that is approximately 20 ft in length and 3 1/4 in. in diameter with a poisoned length of about 15 ft. The rod is made in four segments that are supported by an internal 3/8-in.-diam rod of type 347 stainless steel; the

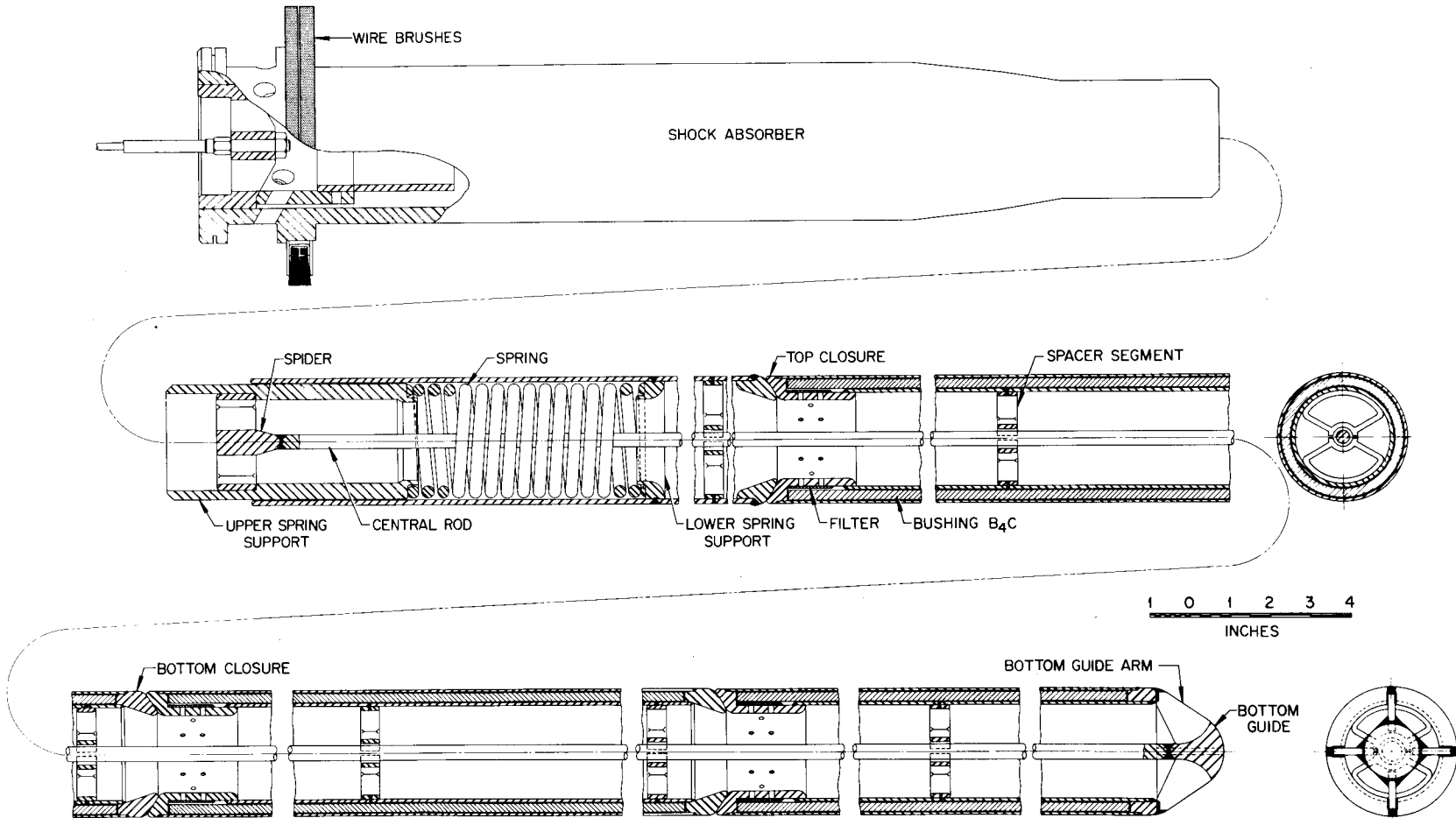


Fig. 3. Details and General Arrangement of Segmented Control Rod.

bottom three segments contain annular rings of hot-pressed B_4C clad with type 304 stainless steel. All surfaces of the stainless steel in contact with the B_4C are copper plated (0.010-in.-thick layer) to prevent the high-temperature reaction, mentioned above, of the boron with the nickel in the steel. Flexibility is achieved by elastic bending of the central rod between spacer support points, with the segments moving relative to one another within the connecting ball-and-socket joints. One face of each of the ball-and-socket joint is overlaid with a 1/16-in. (min) Hastelloy-C weld deposit to prevent self-welding. A woven stainless-steel filter is attached to the top of each poison section to vent the inner volume to the reactor so that no pressure differential will exist across the tubing walls during operation of the reactor. The rod segments are kept in contact by a top Inconel-X compression spring to maintain a leak-tight flow channel for the control rod coolant. This spring and top slip-joint allow for the relative movement of the central support rod and the tubing that will arise from temperature differences occurring during normal rod operation.

Thermal Considerations

Control rod cooling is achieved by a combination of convective and radiative heat transfer. Cool helium flows over the rod drive mechanism, down the shroud, and into the center of the control rod. A wire brush seal is provided between the top of the control rod and the shroud tube to prevent bypassing the cool helium directly into the top plenum of the reactor. This gas absorbs about half of the heat generated in the case of a fully inserted rod and is discharged from the bottom of the rod. The flow then combines with the leakage from the bottom seals and flows either through the control rod channels or between moderator blocks to the top plenum.

The heat removed by thermal radiation amounts to approximately half of the heat generated. A black oxide coating is provided on the outside of the control rod to increase the emissivity of this surface. The heat radiated is absorbed by the graphite and dissipated into the coolant flow in the annulus between the fuel element sleeves and the graphite.

The amount of coolant flow required depends on the ratio of heat generation in the rods, the heat transfer rates obtained, and the maximum allowable temperatures for the control rod components. A plot is shown in Fig. 4 of the stainless steel cladding temperatures as a function of distance into the reactor core for a fully inserted rod operating at the maximum average heat generation of 7500 Btu/hr·ft with a coolant flow of 75 lb/hr. Also shown are plots of the temperatures of the central support rod, the cooling gas, the B₄C, and the graphite surface. These curves were computed on the basis of a top inlet cooling gas temperature of 386°F, which was conservatively estimated (see appendix) from the heat absorbed from the rod drive mechanism, the nozzle, and the shroud tube,

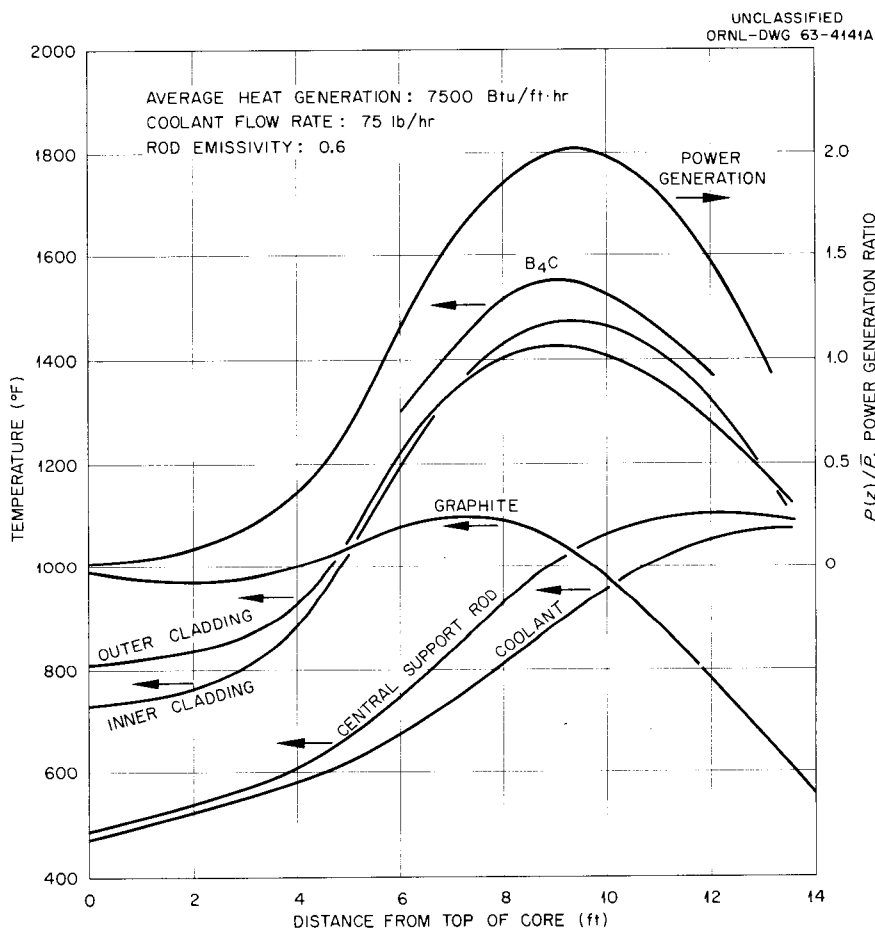


Fig. 4. Control Rod Component Temperatures and Axial Power Distribution in Reactor Core Based on Bank Insertion of All Control Rods to a Depth of 62 in., Coolant Flow of 75 lb/hr, and a Rod Emissivity of 0.6.

assuming that the coolant gas enters initially at a temperature of 125°F. The emissivity of the outer surface of the blackened control rod was taken as 0.6 and that of the graphite wall as 0.8. The graphite temperature profile was taken from an Allis-Chalmer's study.¹¹ The axial heat deposition profile used was taken to be the same as the core power distribution, also shown in Fig. 4, for 62-in. bank insertion of the rods.¹² The temperature drops across the gaps between the B₄C bushings and the stainless steel tubing and across the bushings were allowed for in these calculations. Also, the variations in the gaps caused by differential thermal expansion between the B₄C bushings and the stainless steel as the temperature level changes were considered.

The maximum temperature allowable for continuous operation of the stainless steel in this application is 1600°F. It may be seen from Fig. 4 that, for the maximum average heat generation rate of 7500 Btu/hr·ft of the rod length, a coolant flow rate through the rod of 75 lb/hr is adequate. The 7500 Btu/hr·ft rate represents the maximum average heat generation rate for any control rod and corresponds to the central rod fully inserted. It should be noted that even though the maximum temperature reached under normal operating conditions is about 1475°F, the peak temperature of the structural element (the central support rod) is only 1100°F. The procedures used in obtaining the data of Fig. 4 are described in the appendix.

An examination of the consequences of coolant flow stoppage was made, although this event appears to be unlikely, since spare compressors and heat exchangers are provided in the cooling system. The maximum surface temperature with radiation cooling only is shown in Fig. 5 to be about 2080°F. Since the reactor would be scrammed if the vessel coolant (the source of the control rod coolant) were not available, this temperature would exist only for a short time and should not damage the control rod. The stress developed in the central rod in supporting the weight of the control rod is about 1150 psi, while the yield strength of type 347 stainless steel, even at 2000°F, is 7500 psi, thus giving a safety factor of at least 6.

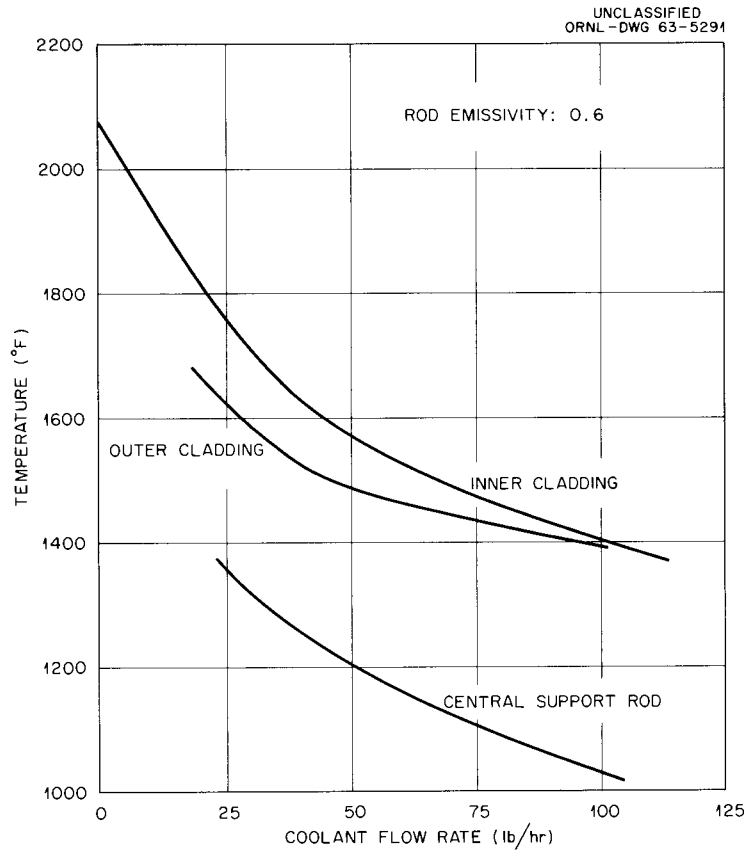


Fig. 5. Effect of Flow Rate on Control Rod Temperatures.

The effect on the peak cladding temperature of varying the stainless steel emissivity was evaluated, and the results are shown in Fig. 6. It may be seen that an emissivity of about 0.25 is required by the 1600°F maximum allowable cladding temperature. If the emissivity were only 0.3 the maximum temperature of the central support rod would be about 1170°F, although the maximum cladding temperature would reach 1570°F. An emissivity of at least 0.6 was readily obtainable with the oxidized surface.¹³

Internal cooling provides a stable flow passage for the coolant, and thus eliminates the problems of external cooling that would be associated with eccentricity of a rod in a channel. However, one source of thermal instability which is difficult to allow for in the design is that of non-uniform heat generation around the circumference of the rod as caused by the radial thermal-neutron flux gradient. This effect was studied to determine whether it would cause appreciable control rod bowing. The

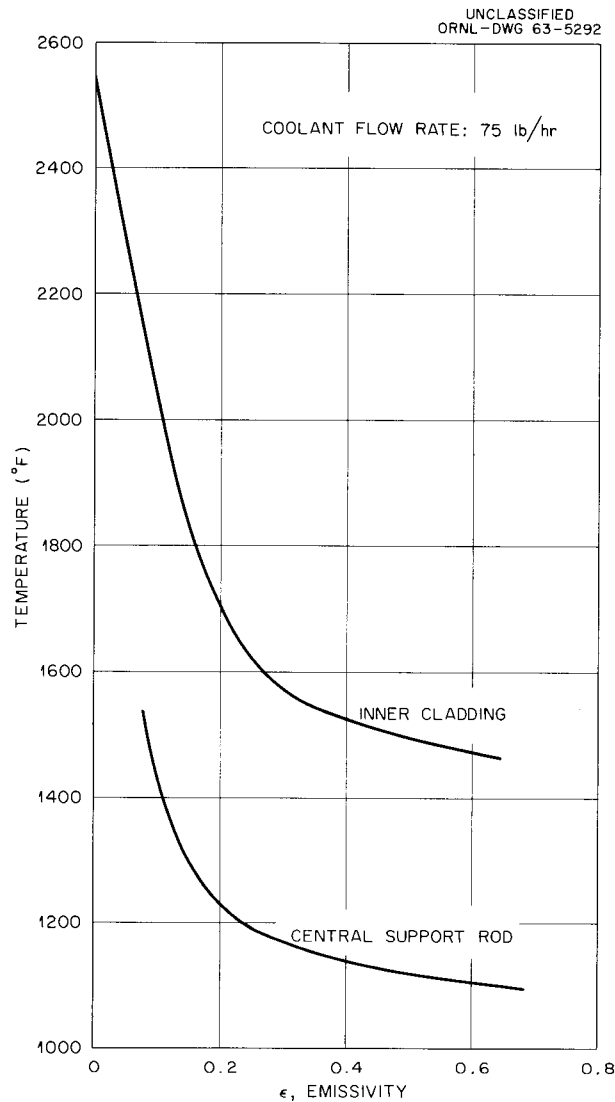


Fig. 6. Effect of Emissivity on Control Rod Temperatures.

maximum unsymmetrical heating will occur in rod P (Fig. 1) with rods C, P, X, and L fully inserted. This heating is described by the following equation:¹⁴

$$\frac{Q(\alpha)}{\bar{Q}} = 1 - 0.1652 \cos \alpha ,$$

where α is the angular position on the circumference and \bar{Q} is the heat generation rate. Based on the equation for the case of heat conduction in a solid with simultaneous internal heat generation and heat loss to

the environment¹⁵ and the above relationship, the following equation for the circumferential temperature variation was derived for the control rod:

$$\Delta t(x) = 8.06 \bar{q}' \left[\frac{1}{6h} - \frac{0.165}{6h + 68} \cos \left(\frac{\pi x}{0.38} \right) \right],$$

where

$\Delta t(x)$ = temperature difference between rod surface and environment
at point x around rod circumference,

\bar{q}' = average linear heat generation rate,

h = heat transfer coefficient

The maximum average temperature variation around the rod circumference was computed to be 181°F. This temperature variation could cause a bow of only 0.255 in. over the length of a 5-ft control rod segment and thus should not cause any difficulty in the operation of the rods.

It was suggested that another difficulty might arise if a portion of the rod were to contact the graphite wall. However, this should not present a problem, since the portion of the rod touching the wall would be cooled, and this should cause it to bow away from the graphite and thus eliminate the contact and hence the cooling effect.

Mechanical Considerations

The 3/8-in.-OD central support rod is the primary structural element of the control rod. This member, the top spider, and the bottom guide are all made of type 347 stainless steel, which was chosen for its superior high-temperature strength characteristics; for example, at 1500°F the yield strength of type 347 stainless steel is approximately twice that of type 304 stainless steel. The support rod was designed to absorb the residual shock load from the shock absorber of a 25-g deceleration force without permanent deformation.¹⁶ Also, this rod will absorb the entire load of a free-falling control rod without failure in the event the shock absorber does not function. The only critical welds in the rod are those that join the top spider and the bottom guide to the central rod, and these

were inspected by both radiography and dye-penetrant methods in the production of the rods.

Selection of the thickness of the cladding was somewhat arbitrary. The outside cladding was made thin, 0.055-in. wall, to reduce neutron reflection but heavy enough to withstand erosion by rubbing (for example, against the shroud tip). The inner cladding wall was made 0.075 in. thick to impart the compressive strength required to resist the stresses that would be encountered during a broken-cable incident.

There will be thermal stresses induced in these tubes by the temperature difference existing during normal operation. The worst case will occur with the lower segment of the central control rod fully inserted. In this case, an average temperature difference of approximately 66°F will exist between the two tubes. This temperature difference will place the inner tube in compression and the outer in tension, with a stress of about 8000 psi, which is well below the yield point for temperature level at this point. The tubing may also be stressed by swelling of the B₄C, although with the internal clearances used this effect should be insignificant.

Each spacer was split into two sections and each section was plug-welded before copper plating to the inside of the inner tube to minimize tube distortion and subsequent assembly difficulties. This arrangement also eliminated any strength discontinuities in the central rod that would have occurred had the spacers been attached to this rod.

The primary considerations with respect to the top spring were the selection of a satisfactory material and an appropriate design for the required movement with sufficient loading. Inconel-X (of proper heat treatment) was chosen for this application because it retains its mechanical properties up to 1100°F.¹⁷ Even in the event of loss of control rod coolant, this spring should function satisfactorily. A spring rate of 50 lb/in. and a total travel of 2 1/4 in. were obtained with 15 1/2 turns of wire (13 1/2 active coils 2 9/32 in. ID, U.S. wire gage 1.0). The rod is assembled with 1-in. precompression and thus allows an additional 1 1/4 in. of travel, which is equivalent to a temperature difference between the central rod and the cladding of 510°F. This gives a safety

factor of about 2 for the normal case of the central rod fully inserted and coolant flow of 75 lb/hr.

Fabrication and Testing of the Mockup Control Rod

A mockup control rod was built to verify the feasibility of assembling the rod and to investigate possibilities of reducing the cost. Also, a limited test program was carried out to establish the coolant pressure drop and to check the extent of the control rod flexibility. Because of the high cost of the B₄C bushings, aluminum machined to give the same overall weight was used as a substitute material. Other simplifications incorporated in the mockup were elimination of the Hastelloy overlay on the ball and socket piece and plug welding of the spacers to the inner can instead of resistance spot welding, as originally planned.

The mockup rod, as first assembled, contained only one spacer at the midpoint of each segment, and the diametral clearance between the central 3/8-in.-diam rod and the spacers was about 1/4 in. The effect of these two items was to make the control rod too flexible, and the segments cocked relative to each other. The rod was reassembled with one additional spacer in each segment just above each joint, and the excessive clearance was eliminated by welding bushings to the central rod at the spacer locations. These revisions achieved the desired degree of stability and rod flexibility, and the appropriate changes were incorporated in the final design. The mockup rod is shown in Fig. 7.

The pressure drop was measured with the rod hanging in a vertical position, as shown in Fig. 8. The test results,¹⁸ given in Fig. 9, show that, for an air flow equivalent to 75 lb of helium per hour, the pressure drop through the rod is about 1.00 lb/ft². The leakage through the top slip joint was equivalent to less than 0.02 lb of helium per hour, and the leakage out of the ball and socket joints was negligible.

The pressure drop measurements were later confirmed by similar tests on a production control rod. The tests indicated that the mockup rod pressure loss was about 10% greater than that for the production rod. It was also shown that about one-half the total loss occurred across the top

UNCLASSIFIED
PHOTO 53805A



16

Fig. 7. Mockup Control Rod.

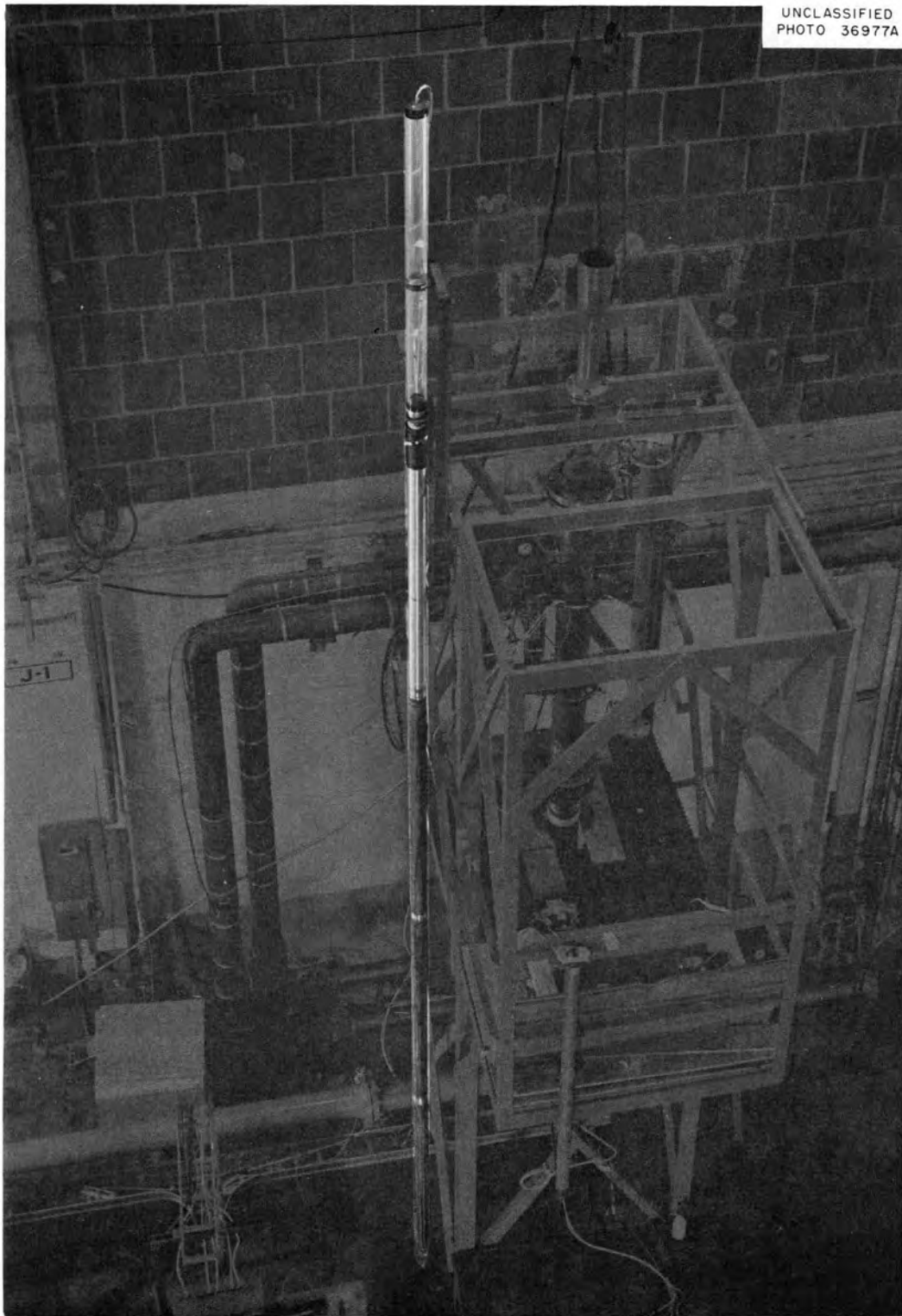


Fig. 8. Test Arrangement for Control Rod Pressure Drop Measurements.

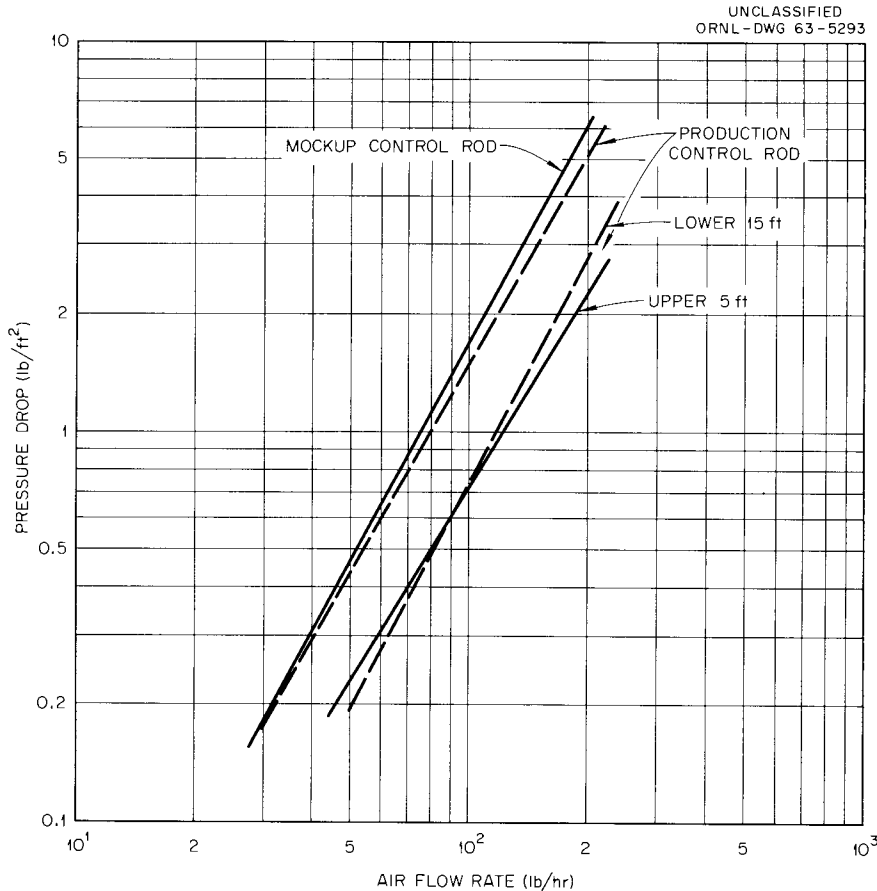


Fig. 9. Results of Pressure Drop Measurements.

5-ft rod segment because of the restricted flow area at the Inconel spring location.

Production of the EGCR Control Rods

The control rods were procured from Dresser Products, Great Barrington, Massachusetts, according to Specification No. EGCR-3, dated March 3, 1961, which was prepared by the Metallurgy Division of the Oak Ridge National Laboratory.¹⁹ Some of the rod components are shown in Figs. 10 through 15. The spacer segments that center the 3/8-in.-diam rod inside the inner tube are shown in Fig. 10. The spacers were plug-welded to the inner tube before the tube was copper plated. The top spider, also shown in Fig. 10, essentially supports the weight of the control rod via the central support rod to which it is welded.

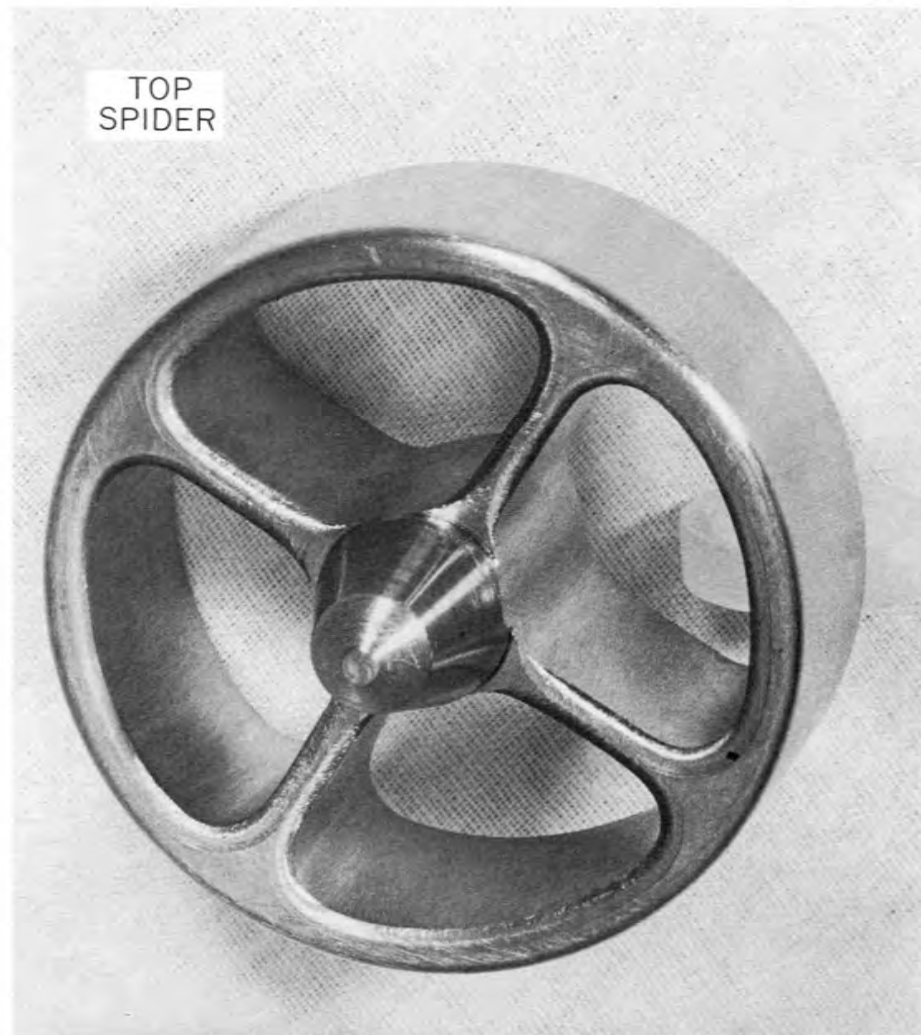
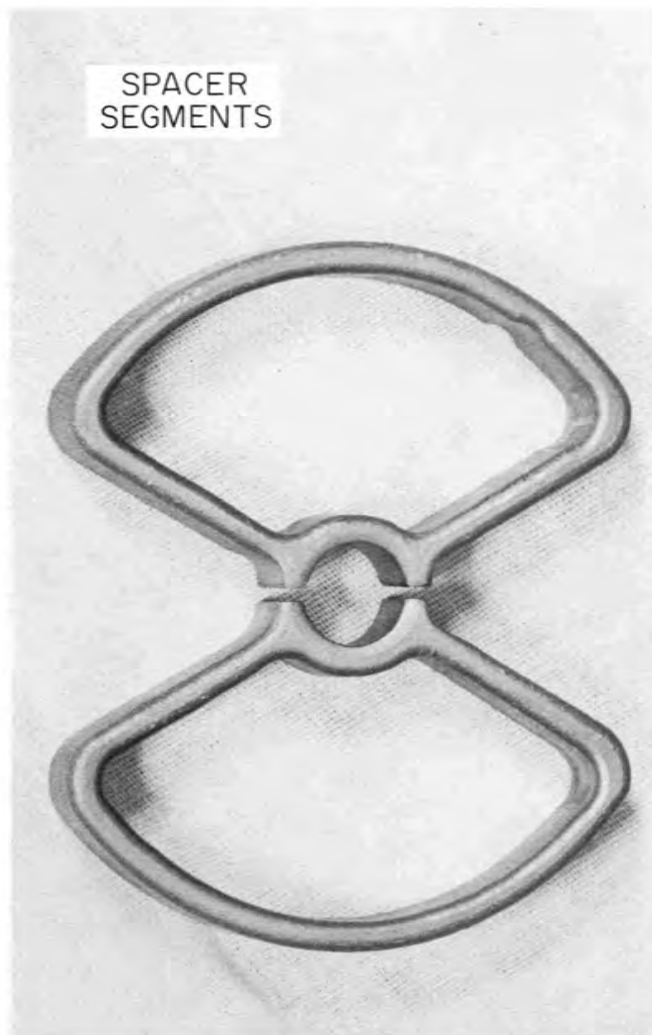


Fig. 10. Top Spider and Spacer Segments.

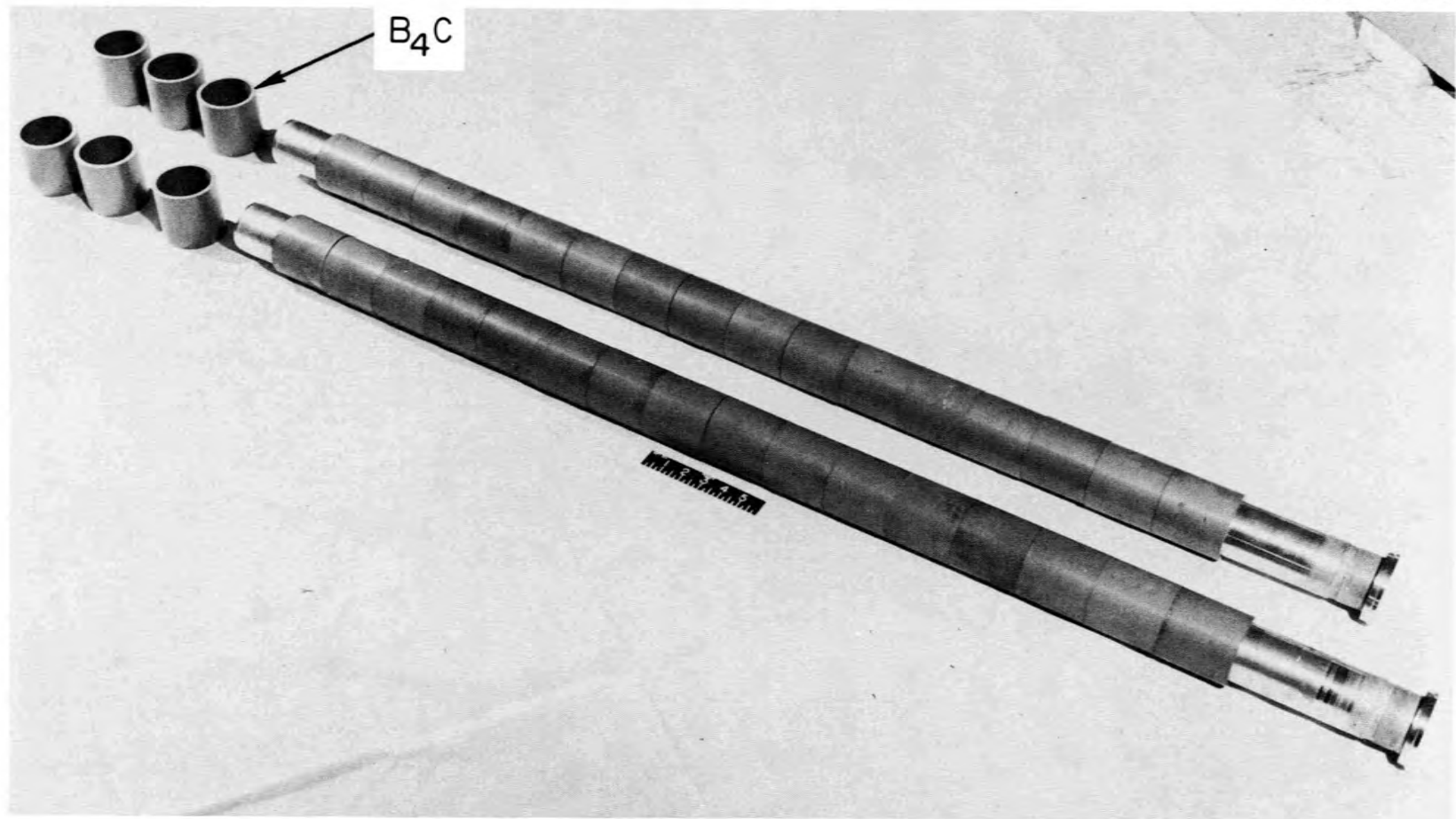


Fig. 11. Partially Assembled EGCR Production Control Rods.

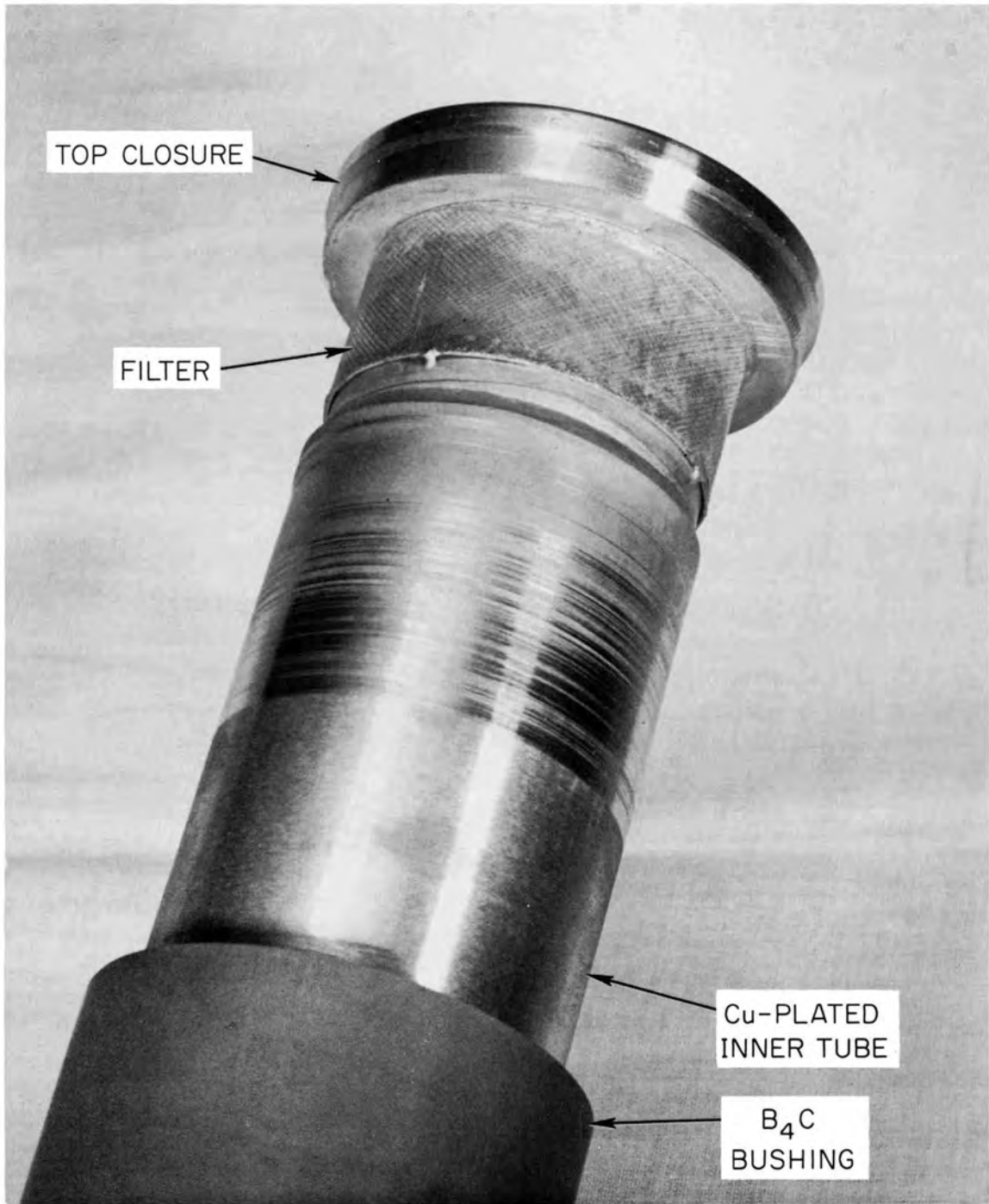
UNCLASSIFIED
PHOTO 62812

Fig. 12. Inner Tube Details.

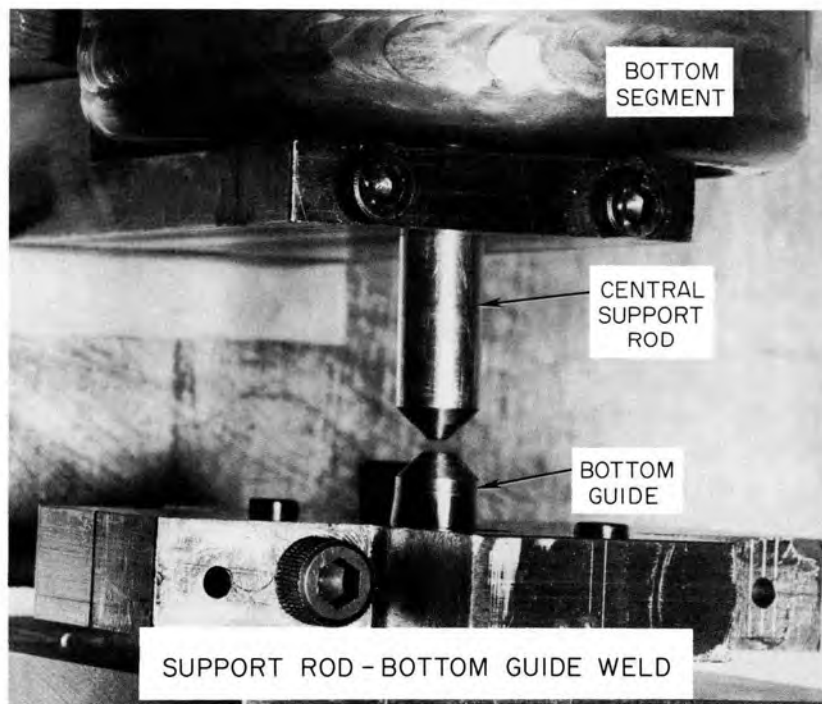
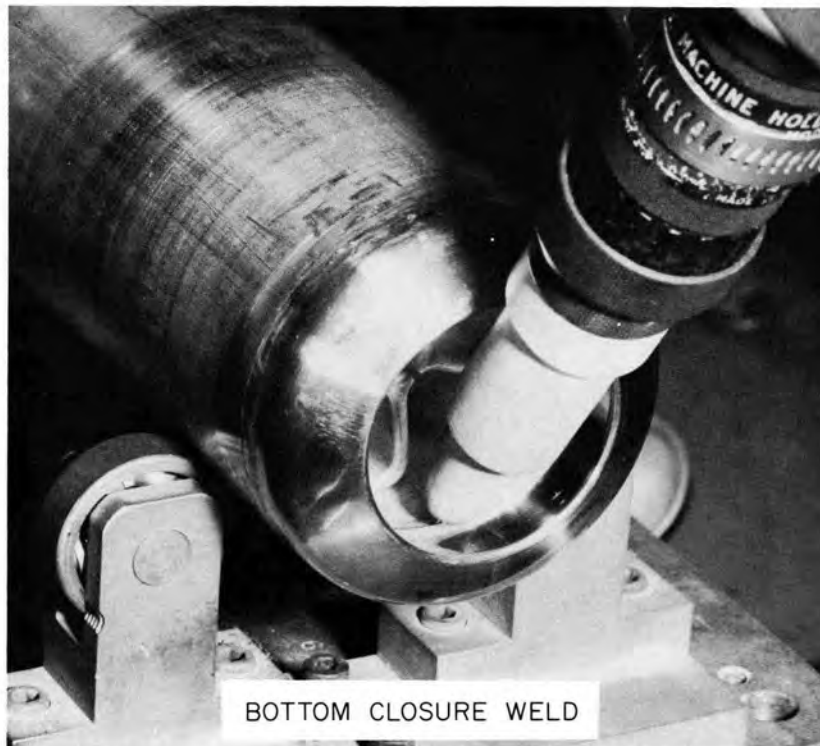
UNCLASSIFIED
PHOTO 62814

Fig. 13. Final Weld on Bottom Closure and Setup for Full Penetration Welding of Support Rod to Bottom Guide.

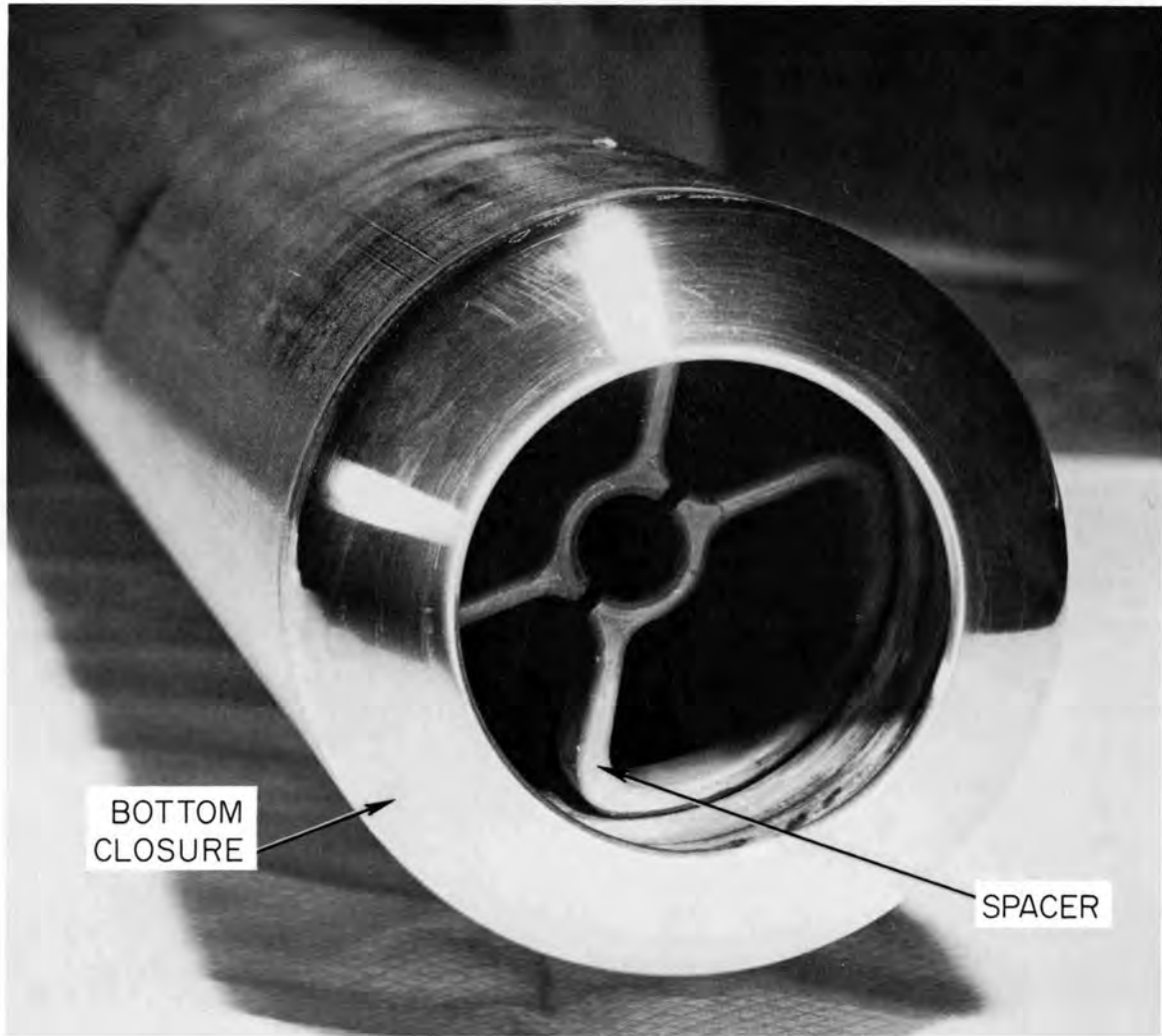


Fig. 14. Segment Spacer in Bottom Closure.

The assembly of the B_4C bushings on the inside rods is indicated in Fig. 11, and the filter details can be seen in Fig. 12. The filter was tack-welded in place on the top closure before the inner tube was attached. The filter was masked off during part of the plating operation so that it received only a 0.003-in. copper plate, while the outer surface of the inner tube received a 0.010-in. plate. Two of the welding operations are shown in Fig. 13: the making of the weld to seal the inner tube to the bottom closure, and the making of the final weld for attaching the bottom

DRESSER PRODUCTS . INC.

UNCLASSIFIED
PHOTO Y-46298

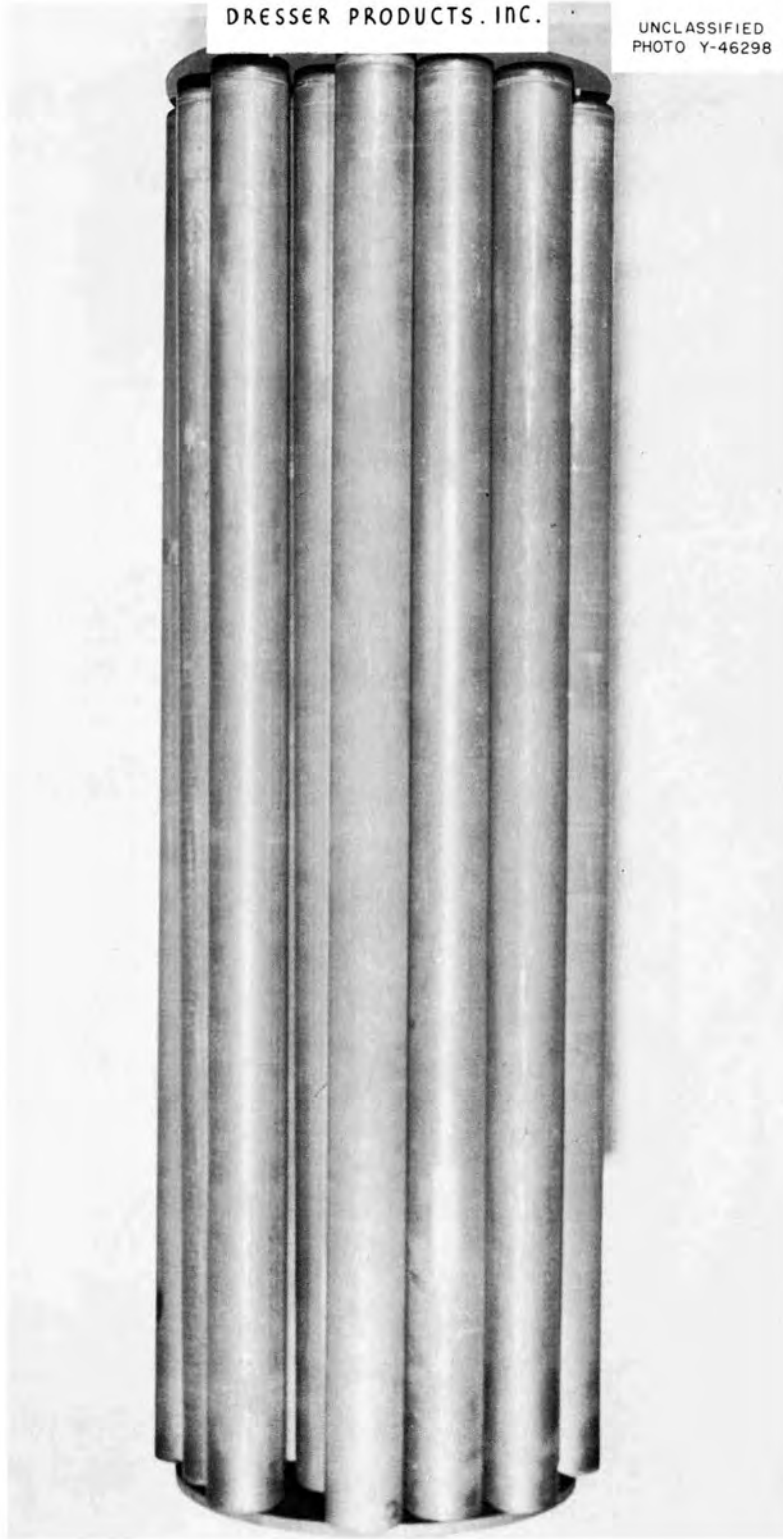
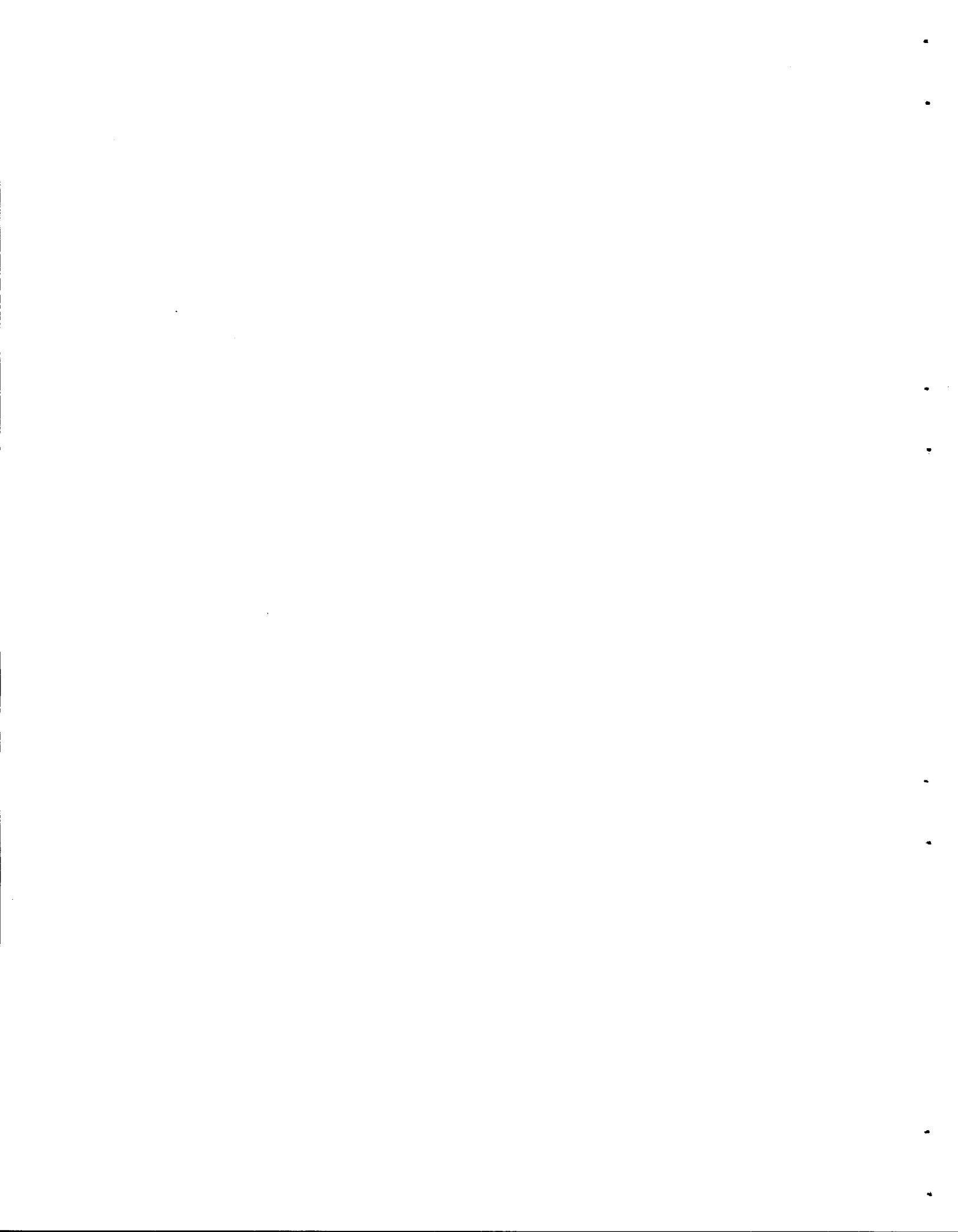


Fig. 15. Fixture for Oxidizing Treatment.

guide piece to the central support rod. The central support rod was temporarily extended for making this weld by compressing the top spring. A completed rod segment with the lower spacers in place is shown in Fig. 14. The fixture for inserting the rod segments into a furnace to perform the surface oxidation treatment is shown in Fig. 15. The completed rod segments containing the B_4C were vapor-blast cleaned, degreased, and heated in wet hydrogen for 4 hr at $1700^\circ F$ to give a surface oxidation designed to yield a high emissivity.

The primary manufacturing problem encountered was the development of satisfactory copper-plating techniques to achieve the thicknesses and tolerances desired, particularly on the inner surface of the outer tube. The final weights of the finished rods varied from 137 to 142 lb and were distributed as follows:

Weight Range (lb)	Number of Rods
137-138	2
138-139	1
139-140	8
140-141	5
141-142	9



References

1. C. A. Preskitt et al., "Physics Analysis for the Design of the EGCR," USAEC Report ORNL-3522, Oak Ridge National Laboratory, to be published.
2. Oak Ridge National Laboratory, "Gas-Cooled Reactor Project Quarterly Progress Report for Period Ending June 30, 1960," USAEC Report ORNL-2964, pp. 43-44.
3. Allis Chalmers Manufacturing Company, "Control Rod Material - Lifetime Prediction and Preliminary Mechanical Design," Job Report No. 3-250-5.0, Feb. 16, 1959.
4. P. Senio and C. W. Tucker, "The Stability of B₄C After 15 (at.) % Burnup, USAEC Report KAPL-1091, Knolls Atomic Power Laboratory, May 15, 1954.
5. W. D. Valovage, "Effect of Irradiation on Hot-Pressed Boron Carbide," USAEC Report KAPL-1403, Knolls Atomic Power Laboratory, Nov. 15, 1955.
6. W. K. Barney et al., "The Use of Boron Carbide for Reactor Control," Nucl. Sci. Eng., 4: 439-448 (1958).
7. W. V. Cummings, "Radiation Effects in Borides," USAEC Report GEAP-3743, Pt. III, General Electric Company, May 1962.
8. Westinghouse Electric Corporation, "Technical Progress Report - Pressurized Water Reactor (PWR) Project, June 24, 1960 to Aug. 23, 1960," USAEC Report WAPD-MPR-81, p. 61.
9. A. F. Gendo and M. W. Mallett, "Solid-Phase Reaction Studies of Control Rod Materials," USAEC Report BMI-1078, Battelle Memorial Institute, March 9, 1956.
10. J. H. Coobs and E. S. Bomar, "Methods of Fabrication of Control and Safety Element Components for the Aircraft and Homogeneous Reactor Experiments," USAEC Report ORNL-1463, Oak Ridge National Laboratory, Feb. 26, 1953.
11. Allis-Chalmers Manufacturing Company, "Temperature Distribution [of] Moderator and Reflector [of] Reactor Core, EGCR," Study No. II-226, Suppl. I, December 1960.

12. Oak Ridge National Laboratory, "Gas-Cooled Reactor Project Quarterly Progress Report for Period Ending September 30, 1960," USAEC Report ORNL-3015, pp. 11-14.
13. W. H. McAdams, Heat Transmission, p. 475, 3rd ed., McGraw-Hill, New York, N.Y., 1954.
14. Oak Ridge National Laboratory, "Gas-Cooled Reactor Project Quarterly Progress Report for Period Ending June 30, 1960," USAEC Report ORNL-2964, pp. 12-14.
15. M. Jakob, Heat Transfer, p. 244, Vol. I, John Wiley and Sons, New York, N.Y., 1958.
16. J. M. Corum, "Structural Analysis of EGCR Control Rods," Jan. 16, 1961, unpublished report.
17. "Spring Materials for High-Temperature Service," Product Engineering, 27: 186-193 (August 1956).
18. Oak Ridge National Laboratory, "Gas-Cooled Reactor Program Progress Report for Period Ending September 30, 1963," USAEC Report ORNL-3523, to be published.
19. Oak Ridge National Laboratory, "Specifications and Drawings for the Control Rods for the Experimental Gas-Cooled Reactor," USAEC Report ORNL-TM-547, May 29, 1963.
20. L. W. Flanigan, G. R. Whitacre, and H. R. Hazard, "Model Studies of Flow and Mixing in the Partially Enriched Gas-Cooled Power Reactor," USAEC Report BMI-1397, Nov. 30, 1959.
21. M. Jakob, Heat Transfer, p. 580, Vol. II, John Wiley and Sons, New York, N.Y., 1957.
22. E. S. Davis, "Heat Transfer and Pressure Drop in Annuli," Trans. ASME, pp. 755-760, October 1943.

Appendix

CALCULATION OF EGCR CONTROL ROD TEMPERATURE PROFILE

The method employed in calculating the axial temperature profile consisted of dividing the rod into 1-ft sections and, by an iteration procedure, determining the heat transferred both by convection to the helium flowing downward inside the rod and by radiation and conduction from the outer rod surface to the graphite. With a known inlet gas temperature, known heat generation rates, and an assumed temperature profile for the graphite, a heat balance across each 1-ft section was obtained before proceeding to the next lower section. Thus the average temperatures in each 1-ft increment were successively determined.

The model used in making the calculations for each 1-ft increment is shown in Fig. A1. It was assumed that the heat was generated in the outer edge of the B_4C . The heat generation rate was obtained from Fig. 4 by averaging the power generation ratios, $P(z)/\bar{P}$, for each increment and multiplying by the rod average heat generation rate. The maximum average value of 7500 Btu/hr.ft was used, since it applied to the condition with the central rod (position N of Fig. 1) fully inserted.

The general calculational procedure followed to obtain the rod temperature profile is summarized below, and a numerical example is given in a later section:

1. The value of Q_C , heat removed by convection, was assumed, and \bar{t}_g , the average gas temperature, was computed based on the known inlet gas temperature.
2. The convective heat transfer coefficient, h , on the inner stainless steel cladding was computed using \bar{t}_g and the assumed flow rate w .
3. The heat transfer film temperature drop, Δt_f , and the stainless steel inner tube temperature were calculated.
4. The central support rod temperature was computed by assuming that heat is radiated to the rod from the inner stainless steel tube and then removed from the rod by convection.

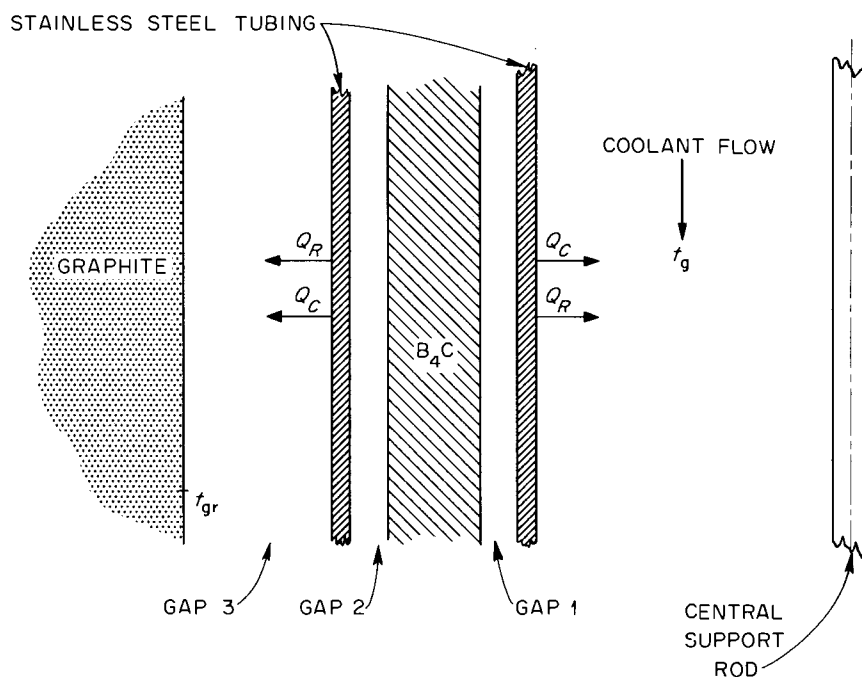


Fig. A1. Model Used for Calculating the Control Rod Temperature Profile.

5. The average gas temperature, \bar{t}_g , was recomputed using the sum of the assumed Q_C and the heat transferred to the support rod, Q_{rod} , and steps 2 through 4 were repeated.

6. The temperature drop across gap 1, Δt_{g-1} , and the B₄C inner surface temperature were computed based on no temperature drop across the stainless steel wall and heat transfer both by radiation and by conduction across the gap.

7. The temperature drop across the B₄C, Δt_{B_4C} , and the B₄C outer surface temperature were computed.

8. The temperature drop across gap 2, Δt_{g-2} , was computed using the value of Q_R found from

$$Q_R = Q_G - (Q_C + Q_{rod}) ,$$

where Q_R is the heat removed by radiation to the graphite, Q_G is the heat generated in the B₄C primarily by neutron absorptions, Q_C is the heat removed by convection, and Q_{rod} is the heat transferred to the central

support rod by radiation. Over the top five 1-ft increments the heat is actually transferred from the graphite to the helium coolant, so

$$Q_R = (Q_C + Q_{rod}) - Q_G .$$

The temperature of the outer surface of the stainless steel cladding was then obtained from the computed value of Δt_{g-2} .

9. The graphite temperature, t_{gr} , and the cladding outer surface temperature, with assumed emissivities, were used to compute Q_R . If the value of Q_R did not correspond with the value found in step 8, a new value of Q_C was assumed and the entire procedure was repeated.

10. After satisfactory agreement was reached using \bar{t}_g for this 1-ft increment, the inlet temperature for the next lower segment was computed and the calculations were repeated for the next lower increment.

The nomenclature and symbols used in the calculations are summarized in the following lists.

Nomenclature

A	Area, ft ²
C_p	Heat capacity, Btu/lb. °F
D	Diameter, ft
\mathfrak{F}	Dimensionless factor for gray surfaces
\bar{F}	Dimensionless geometrical factor for black surfaces
G	Mass velocity, lb/ft ² ·hr
h	Heat transfer coefficient for convection (unless modified by subscript), Btu/hr·ft ² ·°F
k	Thermal conductivity, Btu/ft·°F
L	Length, ft
l	Wall thickness or gap width, ft
Pr	Prandtl number, $C_p \mu / k$
$P(z)/\bar{P}$	Ratio of local power generation rate at axial position z to average power generation rate
r	Radius
Re	Reynolds number
t	Temperature, °F
\bar{t}	Average temperature, °F

T	Absolute temperature, °F
$\Delta t, \Delta T$	Temperature difference, °F or °R
δt	Temperature rise in gas, °F
U	Overall heat transfer coefficient, Btu/hr·ft ² ·°F
w	Flow rate, lb/hr

Greek symbols

ϵ	Emissivity
μ	Viscosity

Subscripts

B ₄ C	Refers to B ₄ C bushings
C	Convection
cond	Conduction
e	Equivalent
f	Film
g	Gas
g-1	Gap 1 (see Fig. A1)
g-2	Gap 2 (see Fig. A1)
g-3	Gap 3 (see Fig. A1)
G	Refers to internal heat generated
gr	Graphite
i	Inside
m	Mean
o	Outside
R	Radiation
R-1	Radiation across gap 1
R-2	Radiation across gap 2
R-3	Radiation across gap 3
rod	Refers to the central support rod
s	Shroud
ss-1	Inner stainless steel cladding
ss-2	Outer stainless steel cladding
T	Total
w	Wall

Coolant Gas Inlet Temperature

It was first necessary to determine the temperature of the coolant gas at the entrance to the B_4C heat-generating portion of the control rod. This gas enters the top of the control rod nozzle at $125^\circ F$, flows downward over the rod drive mechanism, around the concrete shield plug, and into the top of the shroud. For a fully inserted control rod, the gas would then flow down the length of the shroud into the top of the rod through the 1.5-ft length of the shock absorber adaptor and finally through the top 5-ft tube section of the rod before reaching the B_4C -containing sections of the rod. The gas temperature increase caused by absorbing the heat from the drive mechanism, assuming that all the 400-w input is absorbed, amounts to only $8.7^\circ F$. The top portion (~ 12 ft) of the control rod nozzle is cooled on the outside by air at approximately $80^\circ F$ from the service machine room, and the bottom 4 ft is extremely insulated and cooled by the vessel coolant flow at approximately $500^\circ F$ inside. There is a $1/2$ -in. thickness of reflective insulation inside the vessel coolant flow passage and, since the shroud tube is contained within this insulation, the rod coolant flow receives essentially no heat in flowing through this section. Allowing for some heat pickup from the concrete plug, the gas temperature at the level of the inside of the top of the pressure vessel was conservatively assumed to be $150^\circ F$, which is equivalent to absorbing additional heat at a rate of 2500 Btu/hr.

In order to compute the temperature rise of the gas as it flows downward through the hot shroud tube, it was first necessary to estimate the heat transfer coefficient on the outer surface of the shroud, which is exposed to the reactor outlet gas at $1050^\circ F$. Based on model tests,²⁰ the gas from the fuel channels flows upward parallel to the shroud tubes at a velocity computed by assuming (1) that the average flow in a central fuel channel is 2200 lb/hr and (2) that since there are nine fuel channels per control rod position, the flow upward around one control rod shroud is 9×2200 or 19,800 lb/hr.

Since the control rods are placed on 2-ft centers, the area open to flow, as indicated in Fig. A2, is

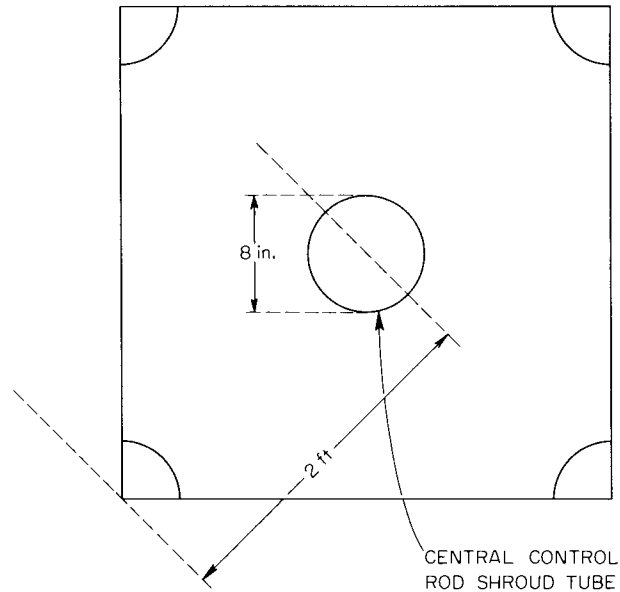
UNCLASSIFIED
ORNL - DWG 63-5294

Fig. A2. Section of Shroud Grid - Plan View.

$$A = 1.415 \times 2.829 \frac{\pi}{4} (0.666)^2 = 3.65 \text{ ft}^2 ,$$

and the mass velocity is

$$G = \frac{W}{A} = \frac{19,800}{3.65} = 5425 \text{ lb/ft}^2 \cdot \text{hr} .$$

The heat transfer coefficient for convection was determined from the following equation:²¹

$$h = 0.03 \frac{k}{L} \text{Re}^{0.8} ,$$

where $\text{Re} = LG/\mu$. It was found that for $L = 10 \text{ ft}$, μ at $1050^\circ\text{F} = 0.0967 \text{ lb/ft} \cdot \text{hr}$, and k at $1050^\circ\text{F} = 0.18 \text{ Btu/hr} \cdot \text{ft} \cdot ^\circ\text{F}$,

$$\text{Re} = \frac{10 \times 5425}{0.0967} = 333,000 ,$$

$$\text{Re}^{0.8} = 26,100 ,$$

and

$$h = 0.03 \times \frac{0.18}{10} \times 26,100 = 14.0 \text{ Btu/hr}\cdot\text{ft}^2\cdot\text{°F} .$$

The inner surface heat transfer coefficient was obtained by using the Dittus-Boelter equation:

$$h = 0.023 \frac{k}{D} \text{Re}^{0.8} \text{Pr}^{0.4} ,$$

where $\text{Re} = 4w/\pi D\mu$ and $\text{Pr} = C_p \mu/k$. The shroud inner diameter (d) is 7.2 in. or 0.6 ft and, using 125 lb/hr for the flow rate (w), 0.06 lb/ft·hr for the viscosity (μ) evaluated at 300°F, then,

$$\text{Re} = \frac{4 \times 125}{\pi \times 0.6 \times 0.06} = 4430 ,$$

$$\text{Re}^{0.8} = 823 ,$$

and, using $k = 0.109 \text{ Btu/ft}\cdot\text{°F}$, which makes $\text{Pr}^{0.4} = 0.872$,

$$h = 0.023 \times \frac{0.109}{0.6} \times 823 \times 0.872 = 3.0 \text{ Btu/hr}\cdot\text{ft}^2\cdot\text{°F} .$$

The overall heat transfer coefficient, U , based on the inside area of the shroud was determined from:

$$\frac{1}{U} = \frac{1}{h_i} + \frac{1}{\frac{k_s \bar{A}}{l_s A_i}} + \frac{1}{h_o \frac{A_o}{A_i}} ,$$

where

h_i = inner surface convective heat transfer coefficient,

h_o = outer surface convective heat transfer coefficient,

k_s = thermal conductivity of the stainless steel shroud, taken as 10 Btu/ft·°F,

l_s = shroud wall thickness, $0.375/12 = 0.031 \text{ ft}$,

\bar{A} = average heat transfer area of shroud,

A_i = shroud inner surface heat transfer area per ft,

A_o = shroud outer surface heat transfer area per ft;

thus

$$\frac{1}{U} = \frac{1}{3} + \frac{1}{\frac{10}{0.031} \frac{7.6}{7.2}} + \frac{1}{14 \frac{8.0}{7.2}}$$

or

$$U = 2.52 \text{ Btu/hr}\cdot\text{ft}^2\cdot^\circ\text{F} .$$

A stepwise calculation was then performed to obtain the gas temperatures for successive 1-ft sections of the shroud using the following equations:

$$Q_c = Q_g ,$$

(convective heat transferred = heat absorbed by the coolant gas) or

$$U A_s \Delta t_m = w C_p \delta t ,$$

where

A_s = shroud heat transfer area, per foot of length,

$$\pi \times 0.6 \times 1 = 1.885 \text{ ft}^2,$$

Δt_m = average temperature of gas outside the shroud (1050°F) less the inside average gas temperature,

δt = gas temperature rise ($t_2 - t_1$) over the 1-ft section,

t_1 = inlet temperature to section,

t_2 = outlet temperature from section,

C_p = helium specific heat, 1.25 Btu/lb·°F;

thus

$$2.52 \times 1.885 \Delta t_m = 125 \times 1.25 \delta t$$

or

$$4.75 \left(1050 - \frac{t_1 + t_2}{2} \right) = 156.25 (t_2 - t_1) .$$

Solving for t_2 gives

$$t_2 = 0.97 t_1 + 31.4 .$$

Using this final equation, the gas temperature at the inlet to a fully inserted control rod was found to be 386°F, and the average temperature of the shroud tube was found to be 933°F.

The flow splits at the top of the control rod with 75 lb/hr flowing down the rod and 50 lb/hr flowing around the outside of the rod, over the shock absorber collet, and then out into the upper plenum. It was assumed that no additional temperature increase would occur as the gas flowed through the 1 1/2-ft-long shock absorber section but that heat would be transferred from the hot upper grid structure and graphite to the coolant as it flowed down the top pipe section of the control rod. This temperature rise was computed using the model shown in Fig. A3.

The following assumptions were made:

1. The upper grid and graphite temperatures are constant at 1000°F.
2. Heat is transferred from the hot surface to the control rod by radiation and conduction through the helium gap.
3. All the heat transferred is absorbed by the coolant flow.
4. The length of rod over which this heat is transferred (4 ft) is divided into 1-ft segments across which average temperatures are used to successively compute the gas temperature rise.

The total heat transferred was determined from

$$Q_T = Q_R + Q_{\text{cond}} = Q_g ,$$

where

- Q_R = heat transferred by radiation,
- Q_{cond} = heat transferred by conduction,
- Q_g = heat absorbed by the coolant gas, helium, flowing down inside the control rod.

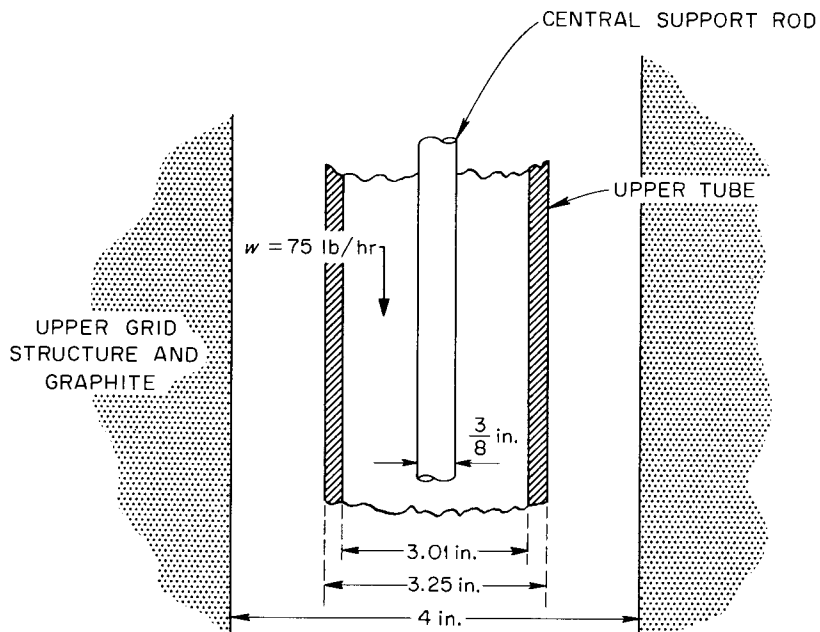


Fig. A3. Model Used to Obtain Temperature Rise in Coolant at Top Section of Control Rod.

Since,

$$Q_g = wC_p \delta t ,$$

$$W = 75 \text{ lb/hr} ,$$

$$C_p = 1.25 \text{ Btu/hr}\cdot^\circ\text{F} ,$$

it is found that

$$Q_g = 75 \times 1.25 \delta t = 93.75(t_2 - t_1) ,$$

where

t_1 = gas inlet temperature for each 1-ft section,

t_2 = gas outlet temperature for each 1-ft section.

Now, since

$$Q_T = UA_w \Delta t_m ,$$

where

$$A_w = \text{inner pipe surface per foot} = \pi \frac{3.01}{12} \times 1 = 0.788 \text{ ft}^2,$$

$$\Delta t_m = \text{mean temperature difference between the graphite and the average coolant gas temperature, } \bar{t}_g,$$

$$= 1000 - \bar{t}_g = 1000 - \frac{t_1 - t_2}{2},$$

U = overall heat transfer coefficient based on the inner pipe wall surface,

and, since

$$Q_T = Q_g,$$

then

$$0.788 U \left(1000 - \frac{t_1 + t_2}{2} \right) = 93.75 (t_2 - t_1)$$

or

$$t_2 = \frac{\left(\frac{119}{U} - 0.5 \right) t_1 + 1000}{\frac{119}{U} - 0.5}.$$

The value of U was found from

$$\frac{1}{U} = \frac{1}{h_w} + \frac{1}{\frac{k_w \bar{A}_w}{l_w A_i}} + \frac{1}{h_{\text{cond}} \frac{\bar{A}_g}{A_i} + h_R \frac{A_{gr}}{A_i}},$$

where

A_i = inner surface area of 1-ft length of the pipe, ft^2 ,
 h_w = inner wall convective heat transfer coefficient,
 k_w = thermal conductivity of the stainless steel pipe wall = 10
 Btu/hr·ft·°F,

- l_w = wall thickness = $0.121/12 = 0.01$ ft,
 \bar{A}_w = average area of a 1-ft length of the wall, ft²,
 \bar{A}_g = average heat transfer area of a 1-ft length of the gap, ft²
 h_{cond} = heat transfer coefficient for conduction across gap 3,
 \bar{A}_{g-3} = average heat transfer area across gap-3, ft²,
 h_R = effective radiation heat transfer coefficient,
 A_{gr} = area of 1-ft length of the graphite channel, ft².

The value of h_{cond} was found from,

$$h_{\text{cond}} = \frac{k}{l},$$

where

k = thermal conductivity of helium at the average gap temperature,
 assumed to be 0.176 Btu/hr·ft·°F,

l = gap width, $0.375/12 = 0.031$ ft;

or

$$h_{\text{cond}} = \frac{0.176}{0.031} = 5.64 \text{ Btu/hr}\cdot\text{ft}^2\cdot\text{°F}.$$

The value of h_w was determined from the Dittus-Boelter equation using
 $k = 0.121$ Btu/ft·°F, $D = 2.635/12 = 0.220$ ft, and $Re = 5100$;

$$h_w = 0.023 \times \frac{0.121}{0.220} (5100)^{0.8} (0.872) = 10.0 \text{ Btu/hr}\cdot\text{ft}^2\cdot\text{°F}.$$

The value of h_R was determined as follows: The heat transferred by radiation is,

$$Q_R = 0.173 \times 10^{-8} \mathfrak{F} A_{\text{gr}} (T_{\text{gr}}^4 - T_w^4),$$

where

$$\mathfrak{F} = \frac{1}{\frac{1}{\bar{F}} + \left(\frac{1}{\epsilon_{\text{gr}}} - 1 \right) + \frac{A_{\text{gr}}}{A_w} \left(\frac{1}{\epsilon_w} - 1 \right)},$$

\bar{F} = dimensionless geometrical factor to allow for net radiation between black surfaces,

ϵ = emissivity,

A_{gr} = graphite nominal surface area per foot of channel length = $\pi \times \frac{4}{12} \times 1 = 1.05 \text{ ft}^2$.

The subscript w refers to the outer surface of the stainless steel pipe and the subscript gr refers to the hot upper grid and graphite surfaces surrounding the pipe section of the control rod. Since

$$T_{gr}^4 - T_w^4 = \Delta T_{g-3} T_{gr}^3 \left(2 - \frac{\Delta T_{g-3}}{T_{gr}} \right) \left[2 - \frac{2\Delta T_{g-3}}{T_{gr}} + \left(\frac{\Delta T_{g-3}}{T_{gr}} \right)^2 \right],$$

where

$$\Delta T_{g-3} = T_{gr} - T_w,$$

and

$$h_R = 0.173 \times 10^{-8} \sigma T_{gr}^3 f \left(\frac{\Delta T_{g-3}}{T_{gr}} \right),$$

where

$$f \left(\frac{\Delta T_{g-3}}{T_{gr}} \right) = \left(2 - \frac{\Delta T_{g-3}}{T_{gr}} \right) \left[2 - \frac{2\Delta T_{g-3}}{T_{gr}} + \left(\frac{\Delta T_{g-3}}{T_{gr}} \right)^2 \right],$$

then

$$Q_R = h_R A_{gr} \Delta T_{g-3}.$$

By taking:

$$\begin{aligned} \bar{F} &= 1, \\ \epsilon_{gr} &= 0.8, \\ \epsilon_w &= 0.3, \\ T_{gr} &= 1460^\circ\text{R}, \end{aligned}$$

$$F = \frac{1}{1 + \left(\frac{1}{0.8} - 1\right) + \frac{4}{3.25} \left(\frac{1}{0.3} - 1\right)} = 0.243 ,$$

it is found that

$$h_R = 1.307 f \left(\frac{\Delta T_{g-3}}{T_{gr}} \right) \text{ Btu/hr}\cdot\text{ft}^2\cdot\text{°F} .$$

Now, U may be found using

$$\frac{\bar{A}_w}{A_i} = \frac{3.13}{3.01} ,$$

$$\frac{\bar{A}_{g-3}}{A_i} = \frac{3.62}{3.01} ,$$

$$\frac{A_{gr}}{A_i} = \frac{4.00}{3.01} ,$$

which gives

$$\frac{1}{U} = \frac{1}{10.0} + \frac{1}{\frac{10}{0.01} \times \frac{3.13}{3.01}} + \frac{1}{5.64 \times \frac{3.62}{3.01} + 1.307 f \left(\frac{\Delta T_{g-3}}{T_{gr}} \right) \frac{4.00}{3.01}} .$$

The value of U from this equation was plotted against ΔT_{g-3} to aid in the iterative calculation using the above equation for t_2 . This procedure required the initial assumption of a value of ΔT_{g-3} to determine U. The adequacy of this assumption was determined as follows:

1. Compute Q_T from $Q_T = 93.75 (t_2 - t_1)$.
2. Find t_w from

$$t_w - \bar{t}_g = \frac{Q_g}{h_w A_1} = \frac{Q_T}{h_w A_1}$$

or

$$t_w = \frac{Q_T}{10 \times 0.788} + \bar{t}_g = 0.127 Q_T + \bar{t}_g .$$

3. Compute ΔT_{g-3} from

$$\Delta T_{g-3} = t_{gr} - t_w = 1000 - t_w .$$

When ΔT_{g-3} from step 3 above agrees with the assumed value, then the value of t_2 found is used as t_1 for the next lower segment, and the entire computation is repeated. This procedure gave a gas temperature at the entrance to the B_4C containing portion of the control rod of $475^\circ F$.

Graphite Temperature Profile

Before proceeding with the computation of the control rod temperature profile, it was necessary to establish the axial graphite temperature distribution based on a study conducted by Allis-Chalmers Manufacturing Co.¹¹ The temperature profile given for graphite column 0 for 62-in. bank insertion of the control rods and a moderator annulus flow rate of 103 lb/hr were used. The temperature profile is shown in Fig. 4.

Sample Calculations

The calculational procedure is illustrated below according to steps 1 through 9 listed above for the 10th segment in which the peak heat generation occurs, i.e., peaking ratio, $P(z)/\bar{P} = 2.01$. The internal heat-generation rate was taken as $Q_G = 2.01 \times 7500 = 15,075$ Btu/hr·ft and the coolant flow rate assumed was $w = 75$ lb/hr.

1. For the calculations of step 1, it was assumed that

$$Q_C = 5800 \text{ Btu/hr}\cdot\text{ft} .$$

The average gas temperature was computed from

$$\bar{t}_g = \frac{1}{2} \frac{Q_c}{wC_p} + t_1 .$$

Using t_2 , the gas outlet temperature as computed (885°F) for the 9th segment for t_1 in the above equation, gives

$$\bar{t}_g = \frac{5800}{2 \times 75 \times 1.25} + 885 = 916^\circ\text{F} .$$

2. In step 2 the stainless steel inner cladding temperature, t_{ss1} , was determined from,

$$t_{ss1} = \frac{Q_c}{h_1 A_1} + \bar{t}_g ,$$

where

h_1 = convective heat transfer coefficient at the inside of the inner tube,

A_1 = heat transfer area per foot of inner tube.

Using the Sieder-Tate equation

$$h_1 = 0.023 \frac{k}{D_e} \text{Re}^{0.8} \text{Pr}^{1/3} \left(\frac{\mu}{\mu_w} \right)^{0.14} ,$$

and for a coolant flow rate of 75 lb of helium per hour,

$$h_1 = \frac{0.7804}{D_e^{0.2} A_1^{0.8} \mu^{0.467}} \frac{k^{2/3}}{\mu^{0.467}} ,$$

or, over the temperature range of interest, allowing for thermal expansion in the dimensional terms, D_e and A_1 , and evaluating k and μ at the average gas temperature of 916°F, the step 2 calculation gives

$$h_1 = 17.95 \frac{k^{2/3}}{\mu^{0.467}} = 16.7 \text{ Btu/hr}\cdot\text{ft}^2\cdot^\circ\text{F} .$$

3. The step 3 calculation then gives

$$t_{ss1} = \frac{5800}{16.7 \times 0.627} + 916 = 1470^\circ\text{F}.$$

4. The central support rod temperature and heat flow from the inner tube to the rod (by radiation) were computed (step 4) as follows:

$$t_{\text{rod}} = \bar{t}_g + \frac{0.173 A_1 \mathfrak{F} \left[\left(\frac{T_1}{100} \right)^4 - \left(\frac{T_{\text{rod}}}{100} \right)^4 \right]}{h_2 A_2},$$

where subscripts 1 and 2 refer to inner surface of the inner cladding and the outer surface of the central support rod, respectively; for $\epsilon_1 = 0.6$ and $\epsilon_2 = 0.3$, $\mathfrak{F} = 0.0604$;

$$A_1 = \pi \frac{2.395}{12} \text{ (per ft of length)} = 0.627 \text{ ft}^2/\text{ft};$$

$$A_2 = \pi \frac{0.375}{12} = 0.0981 \text{ ft}^2/\text{ft}.$$

The convective heat transfer coefficient on the central rod was computed from the following equation²² based on the values of μ and k at 916°F :

$$h_2 = 0.038 \frac{k}{D_1} \left(\frac{D_1 G}{\mu} \right)^{0.8} Pr^{1/3} \left(\frac{\mu}{\mu_w} \right)^{0.14} \left(\frac{D_2}{D_1} \right)^{0.15} = 50 \text{ Btu/hr}\cdot\text{ft}^2\cdot^\circ\text{F}.$$

The equation for the central rod temperature is then

$$t_{\text{rod}} = \bar{t}_g + 0.00133 \left[\left(\frac{T_1}{100} \right)^4 - \left(\frac{T_{\text{rod}}}{100} \right)^4 \right]$$

or

$$t_{\text{rod}} = 916 + 0.00133 \left[(19.31)^4 - \left(\frac{T_{\text{rod}}}{100} \right)^4 \right].$$

This equation was solved by trial and error and gave

$$t_{\text{rod}} = 1033^{\circ}\text{F} .$$

The heat transferred to the rod, Q_{rod} , was obtained from

$$\begin{aligned} Q_{\text{rod}} &= h_2 A_2 (t_{\text{rod}} - \bar{t}_g) \\ &= 4.9 (1033 - 916) = 673 \text{ Btu/hr} . \end{aligned}$$

5. The average gas temperature, as computed in step 1, was

$$\bar{t}_g = \frac{5800 + 573}{187.5} + 885 = 919^{\circ}\text{F} ,$$

which gave

$$t_{\text{ss1}} = \frac{5800}{16.8 \times 0.627} - 919 = 1472^{\circ}\text{F} ,$$

$$t_{\text{rod}} = 1037^{\circ}\text{F} ,$$

$$Q_{\text{rod}} = 578 \text{ Btu/hr} .$$

The value for Q_{rod} agrees well with the value obtained in step 4. With the use of the new value for t_{ss1} , Δt_{g-1} was computed from

$$\Delta t_{g-1} = \frac{Q_c + Q_{\text{rod}}}{\frac{2\pi k}{\ln\left(\frac{r_2}{r_1}\right)_{g-1}} + h_{R-1} A_{R-1}} ,$$

where

k = thermal conductivity of helium,

$$\ln\left(\frac{r_2}{r_1}\right)_{g-1} = \ln\left[\frac{2.615}{2.565} \times \frac{(1 + 2.5 \times 10^{-6} \delta t)}{(1 + 10 \times 10^{-6} \delta t)}\right] ,$$

r_1 = outside radius (or diameter) of inner stainless steel cladding,

r_2 = inside radius (or diameter) of B₄C bushing,

δt is the temperature rise above ambient based on the average temperature, and 2.5×10^{-6} and 10×10^{-6} are the coefficients of thermal expansion of B₄C and stainless steel, respectively.

The grouping $2\pi k / [\ln(r_2/r_1)]$ was plotted against temperature to facilitate the computation. The heat transfer coefficient for radiation was determined from

$$h_{R-1} = 0.173 \times 10^{-8} \epsilon_{ss} T_{ss1}^3 \left(2 + \frac{\Delta t_{g-1}}{T_{ss1}} \right) \left[2 + 2 \frac{\Delta t_{g-1}}{T_{ss1}} + \left(\frac{\Delta t_{g-1}}{T_{ss1}} \right)^2 \right].$$

For ϵ_{ss} (copper plated) = 0.07 and $\epsilon_{B_4C} = 0.8$, $\epsilon = 0.0679$, or

$$h_{R-1} = 0.1175 T_{ss1}^3 f \left(\frac{\Delta t_{g-1}}{T} \right),$$

and

$$h_{R-1} A_{R-1} = 0.008 T_{ss1}^3 f \left(\frac{\Delta t_{g-1}}{T} \right).$$

The function, $f(\Delta T_{g-1}/T)$, was plotted vs temperature and values for Δt_{g-1} were assumed until the computed Δt_{g-1} checked the assumed value.

For an assumed Δt_{g-1} of 40°F or $\bar{t} = 1492^\circ\text{F}$,

$$\frac{2\pi k}{\ln \left(\frac{r_2}{r_1} \right)_{g-1}} = 160.38$$

and

$$h_{R-1} A_{R-1} = 2.38.$$

Then

$$\Delta t_{g-1} = \frac{5800 + 578}{160.38 + 2.38} = 39.7^\circ\text{F} ,$$

which checks the assumed value.

7. The temperature drop across the B₄C was found from

$$\Delta t_{B_4C} = \frac{Q_C + Q_{rod}}{2\pi k_{B_4C}} = \frac{Q_C + Q_{rod}}{2\pi k_{B_4C}} = 0.0266 \frac{Q_C + Q_{rod}}{k_{B_4C}} .$$

$$\frac{\ln \left(\frac{r_2}{r_1} \right)_{B_4C}}{\ln \left(\frac{3.090}{2.615} \right)}$$

For this example

r_1 = inner diameter of B₄C bushing,

r_2 = outer diameter of B₄C bushing,

$$\Delta t_{B_4C} = 0.0266 \times 6378/5.42 = 31.3^\circ\text{F}.$$

The outer surface temperature of the B₄C is then 1472 + 39.7 + 31.3 or 1543°F.

8. The temperature drop across gap-2 was computed in a similar manner to that used for gap-1. When $t_{gr} > t_{ss1}$,

$$\Delta t_{g-2} = \frac{(Q_C + Q_{rod}) - Q_G}{\frac{2\pi k}{\ln \left(\frac{r_2}{r_1} \right)_{g-2}} + h_{R-2} A_{R-2}} ,$$

or when $t_{gr} < t_{ss1}$,

$$\Delta t_{g-2} = \frac{Q_G - (Q_C + Q_{rod})}{\frac{2\pi k}{\ln \left(\frac{r_2}{r_1} \right)_{g-2}} + h_{R-2} A_{R-2}} ,$$

For this example $t_{gr} < t_{ss1}$ so that,

$$\Delta t_{g-2} = \frac{15,075 - (5800 + 578)}{71.87 + 2.87} = 121^\circ\text{F}$$

or

$$t_{ss2} = 1543 - 121 = 1422^\circ\text{F} .$$

9. The heat radiated from the outer cladding to the graphite, Q_R , was found by using the value of t_{ss2} given above and a value of t_{gr} corresponding to the distance into the core under consideration:

$$Q_R = \left[\frac{2\pi k}{\ln \left(\frac{r_2}{r_1} \right)_{g-3}} + h_{R-3} A_{R-3} \right] (t_{ss2} - t_{gr}) ,$$

where h_{R-3} is defined as above using 0.8 for the emissivity of graphite and 0.6 for the oxidized stainless steel surface. Thus

$$Q_R = (6.15 + 15.07)(1422 - 1015) = 8637 \text{ Btu/hr} ,$$

which confirms, approximately, the original assumption:

$$15,075 - (5800 + 578) = 8687 \text{ Btu/hr} .$$

Results

In addition to the results given in the body of this report, the above-described computational method was used in analyzing several other off-design cases. For example, the axial temperature profiles were computed for:

1. 75-lb/hr coolant flow rate with an outside emissivity of 0.3;
2. coolant flow rates of 50 lb/hr and 100 lb/hr;
3. zero coolant flow or radiation cooling only with assumed emissivity values of 0.6 and 0.3; and
4. effect of emissivity on central support rod temperature.

Results of the computations are shown graphically in Figs. A4, A5, and A6. As may be seen from Fig. A5, the 50-lb/hr coolant flow rate would be more than adequate for 12 rod positions (B, C, D, J, P, V, Y, X, W, R, L, and E), since the maximum heat generation rate for a fully inserted rod in one of these positions is only two-thirds of the value used in the computation. Table A1 summarizes the pertinent results of these computations.

The results presented in Table A1 indicate that a coolant flow of about 45 lb/hr will satisfy the design temperature requirement of 1600°F max. The actual coolant flow rates expected, based on flow-pressure drop tests made with the wire brush flow baffle, indicate that about 80 lb/hr should flow down through the rod, with the design total flow of 125 lb/hr entering the control rod nozzle. Thus a safety factor of nearly two exists to allow for variations in tolerances, temperature, and possible wear of the wire brush.

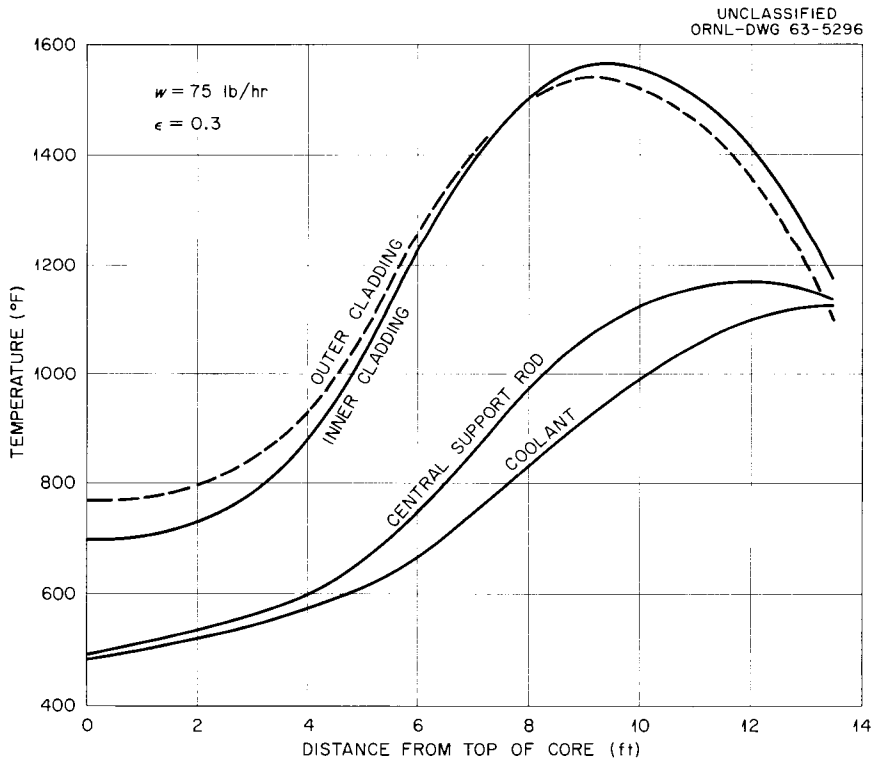


Fig. A4. Control Rod Component Temperatures with a Coolant Flow Rate of 75 lb/hr and a Rod Emissivity of 0.3.

UNCLASSIFIED
ORNL-DWG 63-5297

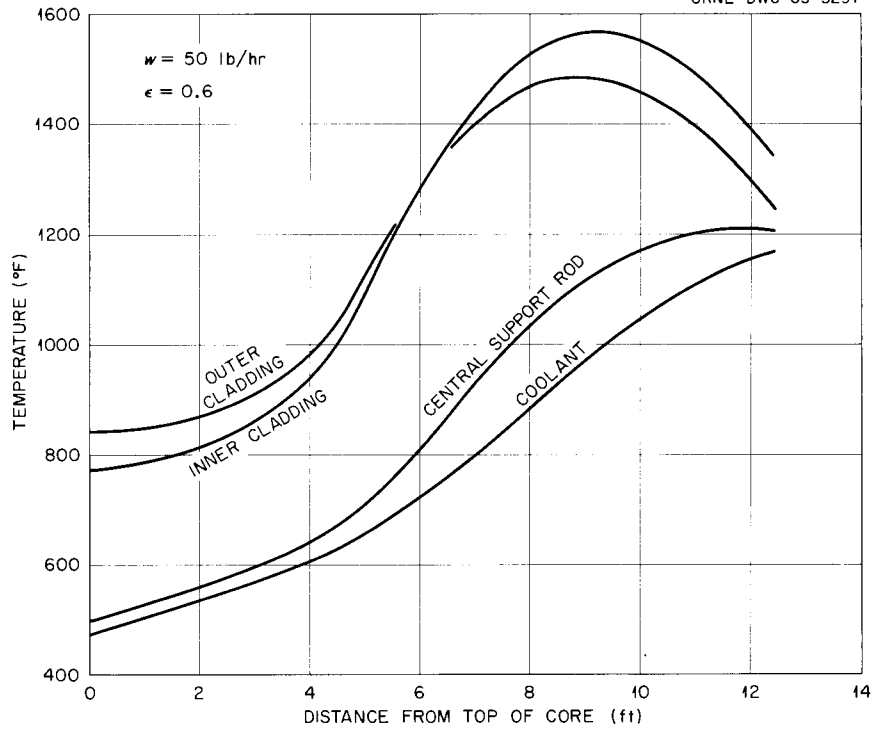


Fig. A5. Control Rod Component Temperatures with a Coolant Flow Rate of 50 lb/hr and a Rod Emissivity of 0.6.

UNCLASSIFIED
ORNL-DWG 63-5298

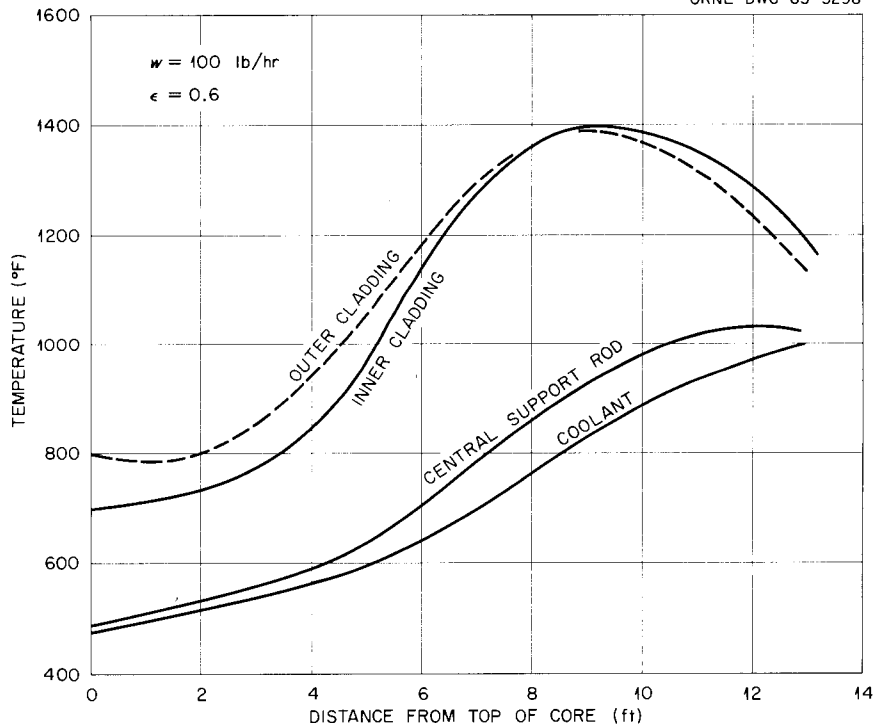


Fig. A6. Control Rod Component Temperatures with a Coolant Flow Rate of 100 lb/hr and a Rod Emissivity of 0.6.

Table A1. Maximum Temperature of Various EGCR Control Rod Components

Flow Rate (lb/hr)	Inner Stainless Steel Cladding (°F)	Outer Stainless Steel Cladding (°F)	Central Support Rod (°F)
0	2080		
50	1565	1485	1210
75	1475	1435	1110
75 ^a	1570	1540	1170
100	1400	1390	1030

^aEmissivity of outer cladding = 0.3.

ORNL-3503

UC-80 - Reactor Technology
TID-4500 (26th ed.)Internal Distribution

- | | |
|----------------------|--|
| 1. S. E. Beall | 87. F. H. Neill |
| 2. W. R. Gall | 88. H. G. O'Brien |
| 3. B. L. Greenstreet | 89. S. A. Rabin |
| 4. A. Goldman | 90. G. Samuels |
| 5. H. L. Hemphill | 91. Ann Savolainen |
| 6. M. R. Hill | 92. M. J. Skinner |
| 7. R. S. Holcomb | 93. J. R. Tallackson |
| 8. M. E. Lackey | 94. W. E. Thomas |
| 9. M. E. LaVerne | 95. J. H. Westsik |
| 10. H. G. MacPherson | 96. R. E. Whitt |
| 11-76. W. D. Manly | 97. F. J. Witt |
| 77. W. R. Martin | 98. F. C. Zapp |
| 78. H. A. McLain | 99-101. Central Research Library |
| 79-84. J. W. Michel | 102-104. Y-12 Document Reference Section |
| 85. S. E. Moore | 105-130. Laboratory Records Department |
| 86. J. F. Murdock | 131. Laboratory Records, RC |

External Distribution

- 132-134. P. D. Bush, Kaiser Engineers
135. R. A. Charpie, UCC Research Administration, New York, N.Y.
136. W. R. Cooper, Tennessee Valley Authority
137-138. David F. Cope, Reactor Division, AEC, ORO
139-140. R. W. Coyle, Vallecitos Atomic Laboratory
141. E. Creutz, General Atomic
142-145. R. B. Duffield, General Atomic
146. H. L. Falkenberry, Tennessee Valley Authority
147. D. H. Fax, Westinghouse Atomic Power Division
148. M. Janes, National Carbon Research Laboratories, Cleveland, Ohio
149. T. Jarvis, Ford Instrument Co.
150. James R. Johnson, Minnesota Mining and Manufacturing Company, Saint Paul, Minn.
151. Richard Kirkpatrick, AEC, Washington
152. C. W. Kuhlman, United Nuclear Corp.
153-154. H. Lichtenburger, General Nuclear Engineering Corp.
155-157. S. Matovich, Allis-Chalmers Mfg. Co.
158. J. P. McGee, Bureau of Mines, Appalachian Experiment Station
159. R. W. McNamee, Manager, UCC Research Administration, New York, New York
160. R. E. Pahler, High-Temperature Reactor Branch, Reactor Division, AEC, Washington

161. H. B. Rahner, Savannah River Operations Office
162. Corwin Rickard, General Atomic
163. M. T. Simnad, General Atomic
164. Nathaniel Stetson, Savannah River Operations Office
165. Donald Stewart, AEC, Washington
166. S. A. Szawlewicz, AEC, Research and Development Branch,
Division of Reactor Development
167. Philip L. Walker, Pennsylvania State University
168. R. E. Watt, Los Alamos Scientific Laboratory
- 169-170. W. L. Webb, East Central Nuclear Group, Inc.
171. C. E. Winters, UCC, Cleveland, Ohio
172. Lloyd R. Zumwalt, General Atomic
173. Division of Research and Development, AEC, ORO
- 174-785. Given distribution as shown in TID-4500 (26th ed.) under Reactor
Technology category (75 copies - OTS)